AD-A127 140 INVESTIGATION OF LIMIT CYCLE RESPONSE OF AERODYNAMIC 1/ /
SURFACES WITH STRUCT..(U) MCDONNELL DOUGLAS
ASTRONAUTICS CO-ST LOUIS MO R P BRILEY ET AL.
UNCLASSIFIED 01 OCT 83 AFOSR-TR-83-0232 F49620-82-C-0043 F/G 20/4 NL

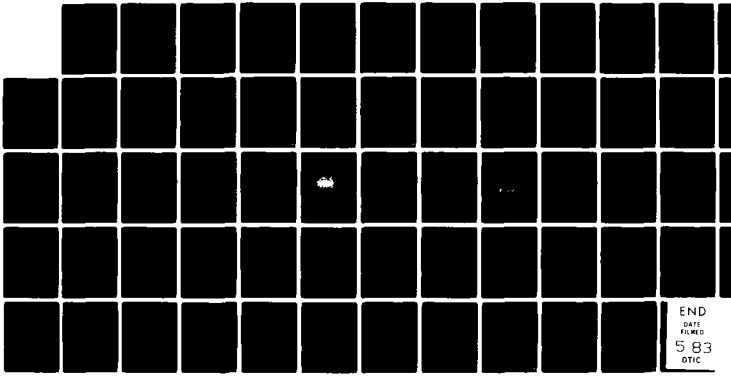

END
DATE FILMED
5 83
DTIC

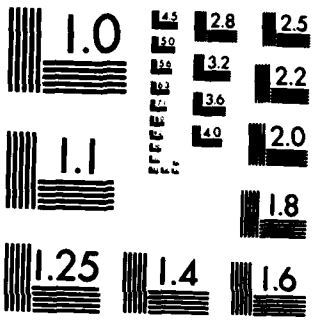

MICROCOPY RESOLUTION TEST CHART
NATIONAL BUREAU OF STANDARDS-1963-A

12

INVESTIGATION OF LIMIT CYCLE RESPONSE OF AERODYNAMIC SURFACES WITH STRUCTURAL NONLINEARITIES

MCDONNELL DOUGLAS ASTRONAUTICS COMPANY-ST. LOUIS DIVISION

MCDONNELL DOUGLAS CORPORATION

INVESTIGATION OF LIMIT CYCLE RESPONSE OF AERODYNAMIC SURFACES WITH STRUCTURAL NONLINEARITIES

Ronald P. Briley

John L. Gubser

19 November 1982

This work was sponsored by

The Air Force Office of Scientific Research

Under Contract Number: F49620-82-C-0043

McDONNELL DOUGLAS ASTRONAUTICS COMPANY-ST. LOUIS
Box 516, Saint Louis, Missouri 63166 (314) 232-0232

McDONNELL DOUGLAS CORPORATION

UNCLASSIFIED

SECURITY CLASSIFICATION OF THIS PAGE (When Data Entered)

REPORT DOCUMENTATION PAGE		READ INSTRUCTIONS BEFORE COMPLETING FORM
1. REPORT NUMBER AFOSR-TR- 83-0232	2. GOVT ACCESSION NO. AD-A127140	3. RECIPIENT'S CATALOG NUMBER
4. TITLE (and Subtitle) Investigation of Limit Cycle Response of Aerodynamic Surfaces with Structural Nonlinearities		5. TYPE OF REPORT & PERIOD COVERED Final Report 1 April 1982-31 October 1982
		6. PERFORMING ORG. REPORT NUMBER
7. AUTHOR(s) R. P. Briley J. L. Gubser		8. CONTRACT OR GRANT NUMBER(s) F49620-82-C-0043
9. PERFORMING ORGANIZATION NAME AND ADDRESS McDonnell Douglas Astronautics Company - St. Louis Division, P.O. Box 516 St. Louis, MO 63166		10. PROGRAM ELEMENT, PROJECT, TASK AREA & WORK UNIT NUMBERS 61102F 2307/B1
11. CONTROLLING OFFICE NAME AND ADDRESS Air Force Office of Scientific Research/NA Bolling Air Force Base Washington, D. C. 20332		12. REPORT DATE 1 October 1982
		13. NUMBER OF PAGES 64
14. MONITORING AGENCY NAME & ADDRESS (if different from Controlling Office)		15. SECURITY CLASS. (of this report) UNCLASSIFIED
		15a. DECLASSIFICATION DOWNGRADING SCHEDULE

16. DISTRIBUTION STATEMENT (of this Report)

Approved for public release; distribution unlimited.

17. DISTRIBUTION STATEMENT (of the abstract entered in Block 20, if different from Report)

18. SUPPLEMENTARY NOTES

19. KEY WORDS (Continue on reverse side if necessary and identify by block number)

Limit Cycle Oscillation
Asymptotic Expansion Method
Structural Nonlinearity

20. ABSTRACT (Continue on reverse side if necessary and identify by block number)

Aerodynamic surface design must often account for the presence of structural nonlinearities induced by freeplay in the support structure and/or control actuators. During this study, application of asymptotic expansion methods to predict the limit cycle behavior of aerodynamic surfaces with structural nonlinearities was investigated. Two basic types of nonlinearities, freeplay and preload, were introduced at the aerosurface support structure and the resulting limit cycle behavior analyzed. The

(see reverse side)

DD FORM 1 JAN 73 1473 EDITION OF 1 NOV 65 IS OBSOLETE

UNCLASSIFIED

SECURITY CLASSIFICATION OF THIS PAGE (When Data Entered)

asymptotic expansion method was used to derive a relationship between the parameters characterizing the structural nonlinearity and the amplitude and frequency of the limit cycle response. First and second order perturbation solutions were obtained to model the "effective" or linearized system parameters governing the nonlinear response of the undamped system.

The results of this investigation show that the asymptotic solutions accurately predict the stationary limit cycle behavior when compared with numerical simulation and describing-function analyses for the nonlinearities considered. The influence of higher harmonics on the predicted limit cycle response were also observed when higher order perturbation solutions were obtained.

The aeroelastic response of a baseline aerodynamic surface was investigated using the asymptotic expansion approach. Flutter results were obtained for the effective system for both rigid and flexible representations of the surface. Steady state aerodynamic loading was assumed in computation of the flutter results. These results were then utilized, in conjunction with the asymptotic solutions, to investigate the interrelationship between the magnitude of the nonlinearity, flight condition and the limit cycle response. Examples and results of the application of the developed solutions are presented.

This study demonstrates the applicability of the asymptotic expansion method in accounting for the influence of structural nonlinearities in the limit cycle analysis of aerodynamic surfaces. Understanding the effects of structural nonlinearities on the dynamic response of systems is important when considerations of stability, response and fatigue life influence the design of the surface support structure and/or actuators.

ACKNOWLEDGMENT

This report was prepared by the McDonnell Douglas Astronautics Company - St. Louis, Missouri, under Contract F49620-82-C-0043, "Investigation of Limit Cycle Response of Aerodynamic Surfaces with Structural Nonlinearities." The program was administered under the direction of Air Force Office of Scientific Research with Dr. Anthony K. Amos as Program Manager.

TABLE OF CONTENTS

LIST OF ILLUSTRATIONS

TITLE

LIST OF ILLUSTRATIONS

TITLE

(Continued)

1.0 INTRODUCTION

Defining the flutter and divergence characteristics of aerodynamic surfaces is a basic requirement to assure structural and performance integrity of a given design in its operational environment. For systems which have structural nonlinearities another mode of aeroelastic response, limit cycle oscillation, may be present. A comparison between limit cycle response and classical flutter and divergence is illustrated in Figure 1. The limit cycle response, Figure 1(c), is defined as a constant amplitude steady state oscillation whereas the divergence, Figure 1(a), and flutter, Figure 1(b), are unstable motions with increasing amplitude. The importance of the limit cycle response is the potential of these oscillations to occur within the flutter and divergence flight envelope. Frequently real hardware designs do have nonlinearities in the surface support structure and/or actuators as a result of manufacturing tolerances and/or freeplay. When these nonlinearities exist, the classical assumption of a linear force-displacement relationship is no longer justified and an understanding of the nonlinear effect on the dynamic behavior is required to evaluate the system response. In this study effort analysis procedures were developed to characterize the limit cycle response of aerosurfaces with discrete structural nonlinearities.

The effects of structural nonlinearities on aerodynamic surface response has been studied both analytically and experimentally, Reference 1 through 5. In these studies several nonlinearities that are typically encountered in aerodynamic surface designs were considered. In the analytical studies of References 1 through 4 the method of harmonic balance or describing-function approach was used to characterize the nonlinear behavior of an aerodynamic surface with root freeplay nonlinearities of the type shown in Figure 2. These nonlinearities are representative of a deadband or "slop" in the root support structure with and without a linear preload. The resulting behavior is such that the stiffness and force developed in the adjacent members is a nonlinear function of amplitude. The describing-function approach uses a one term Fourier Series expansion of the force to account for the effect of this nonlinear stiffness on aerosurface response. This method gave satisfactory

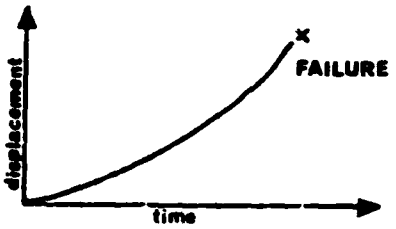

(a) Divergence

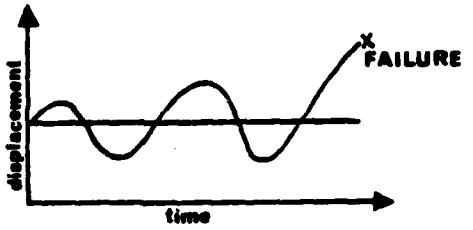

(b) Flutter

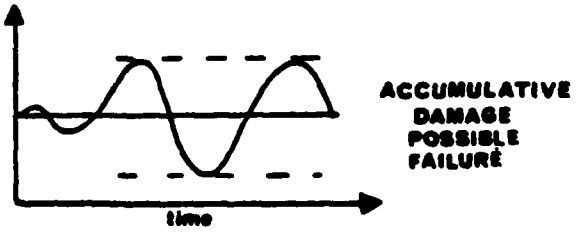

(c) Limit Cycle Oscillation

FIGURE 1 MODES OF AEROSURFACE AEROELASTIC RESPONSE

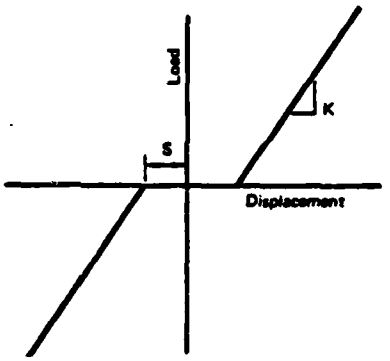

(a) FREEPLAY NONLINEARITY

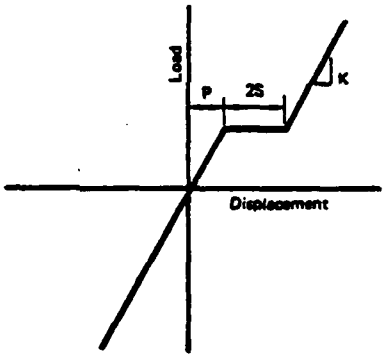

(b) PRELOAD NONLINEARITY

FIGURE 2 TYPES OF STRUCTURAL NONLINEARITIES

results when the amplitude of motion was greater than the magnitude of the freeplay, Figure 2(a), or freeplay plus preload, Figure 2(b). However, it was pointed out References,1 and 2, that when the amplitude of motion is approximately equal to the magnitude of the nonlinearity, significant error can occur as a result of neglecting the higher harmonics in the series expansion of the force-displacement relationship. The truncation of the higher harmonics is an inherent drawback of the one-term describing function approach.

An experimental study of the limit cycle response of aerodynamic surfaces with structural nonlinearities is discussed in Reference 5. During this study a model was developed with root structural behavior which gave a variety of nonlinear stiffness characteristics to the aerosurface. Wind tunnel tests were conducted and data obtained to verify the model's response characteristics. It was noted by the authors of Reference 5 that there exists a need for improved analytical tools to accurately describe the nonlinear behavior in order to better correlate experimental and analytical results

The objective of the present analytical study was to develop a technique to predict limit cycle response of aerosurfaces with discrete structural nonlinearities that retains the flexibility and well defined procedures of the describing-function approach (References 1 and 2) yet provides greater accuracy and generality in modeling the nonlinear system behavior. To meet this objective an asymptotic expansion method was used to model the nonlinear force-displacement relationship that results when nonlinearities of the type shown in Figure 2 are introduced at the aerosurface support. The primary difference between the asymptotic method and the describing-function method is the capability of the asymptotic method to include higher harmonics in the representation of the nonlinearity and obtain successively higher order approximations to the limit cycle response. Using the asymptotic expansion technique a broader category of discrete nonlinearities than those shown in Figure 2 can be modeled.

Specifically, the problem investigated during the present study was the limit cycle response of an aerodynamic surface in a subsonic airstream, Figure 3. The nonlinearities shown in Figure 2 were assumed to act at the root support springs K_θ and K_ϕ shown in Figure 3. This problem is represenative

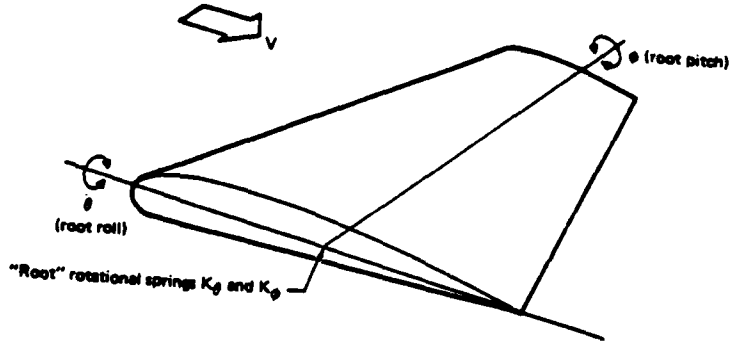

FIGURE 3 AERODYNAMIC SURFACE CONFIGURATION

of a missile control surface with a loose hinge and/or joint slippage in the surface support structure and/or actuator. The aerodynamic forces acting on the surface were modeled using a steady state aerodynamic theory. This theory assumes the lifting force is proportional to and in phase with the torsional motion of the surface which is assumed to be sinusoidal. Simple aerodynamics were used so that the influence of the nonlinearities on the surface response could be evaluated by a much more tractable computational effort. The effects of using a more sophisticated aerodynamic theory for the describing-function approach were investigated and documented in Reference 2. There it was shown that a more sophisticated aerodynamic theory can substantially change the flutter results employed to predict aeroelastic response, but has no impact on modeling the nonlinear behavior. The authors believe that the conclusions presented in Reference 2 are applicable to the present analysis effort as the linear aerodynamic theory does not impact the representations of the structural nonlinearities considered in this study.

This study was organized into two separate tasks. The first task, discussed in Section 2.0, involved development of the asymptotic approximations for the limit cycle response for each of the two nonlinearities shown in Figure 2. First and second order asymptotic solutions were formulated and compared with the results obtained using the describing-function method of References 1 and 2. The equations for including the higher order harmonics in the time history response calculations were also derived under this task. The second task, discussed in Section 3, involved application of the developed asymptotic solutions to predict the limit cycle response of the baseline aerodynamic surface chosen for this study. This baseline surface design is based on the Harpoon missile control surface and is shown in Appendix A. In Appendix A, representative flutter results for selected root spring configurations are presented. These results are used in the applications discussed in Section 3. Appendix B contains the detailed derivation of the asymptotic solutions. While key equations are presented in the text of Section 2, intermediate steps in the derivations are detailed in Appendix B.

2.0 DEVELOPMENT OF ASYMPTOTIC SOLUTION

Application of the method of asymptotic expansions to model nonlinear behavior of an aerodynamic surface response forms the basis of the procedures developed in this investigation. The asymptotic expansion method used is the Krylov-Bogoliubov-Mitropolski (KBM) technique. This technique is a perturbation method based on a more general approach known as the method of averaging, and is discussed in detail in References 6 and 7. In the method of averaging, the motion is assumed to vary slowly with time and the amplitude and phasing are determined as time dependent functions of the system nonlinearities. The advantage of the method of averaging, and in particular the KBM technique, is the stability of the solutions over sufficiently long intervals of time. This type of solution is necessary for quantitative as well as qualitative analysis of the limit cycle behavior of a nonlinear system. Another advantage of the asymptotic expansion technique is that it provides a more accurate determination of the nonlinear load-displacement relationship than the one-term describing-function approach of References 1 and 2, yet can be used in much the same manner. In both the asymptotic and describing-function techniques, the derived expressions for the load-displacement relationship are used to define an "effective" stiffness for the nonlinear element. This effective stiffness is used in subsequent aeroelastic analyses.

The procedures for investigating the limit cycle response developed in this study require defining the flutter characteristics of the aerodynamic surface. In this study, flutter analysis of both rigid and flexible configurations were analyzed. The flutter analysis is performed using the linearized form of the equations of motion, as was done in the describing-function and other methods, References 1 through 4. This approach assumes that an effective stiffness adequately describes the elastic behavior for the infinitesimal oscillations at flutter onset. The details of the flutter analysis for the baseline surface analyzed in this study are presented in Appendix A.

During this study, the nonlinear aeroelastic system was represented by the second order differential equation

$$\frac{d^2x}{dt^2} + \omega_o{}^2 x = \varepsilon f(x) + Q(x) \qquad (1)$$

In Equation (1), $\epsilon f(X)$ represents the nonlinear force acting on the elastic system, X is the surface root displacement, ω_0 is the natural frequency of the linear system (ϵ=0) and Q(x) is the aerodynamic forcing function. The f(X) term appears in Equation (1) as a result of the nonlinear load-displacement relationship for the root support springs of the surface. It is the nonlinear force term that is used to determine the form of the asymptotic expansions derived to approximate the limit cycle response of the nonlinear system.

In the asymptotic method a perturbation technique is used to expand the contribution of the nonlinearity in terms of a small parameter or gage function, ϵ. This expansion takes the form of an asymptotic series comprised of integer powers of ϵ. For the system respresented by Equation (1) the form of the asymptotic solution defined by the KBM technique is given by

$$x = A \cos \psi + \sum_{n=1}^{N} \epsilon^n U_n (A,\psi) + O(\epsilon^{N+1}) \qquad (2)$$

For the freeplay nonlinearity this equation was used directly. For the preload nonlinearity it was modified as will be discussed in Section 2.2. The displacement, X, as defined in Equation (2) consists of a linearly independent combination of periodic functions, the first term being the fundamental harmonic. The remaining terms expanded in powers of ϵ represent the asymptotic approximation of the nonlinear contribution to the response. The functions U_n are periodic functions comprised of higher harmonics of the phasing parameter ψ and the surface root amplitude A. N indicates the order of the asymptotic approximation and the symbol $O(\epsilon^{N+1})$ represents term of order greater than N. A and ψ are, in general, functions of time defined by the ordinary differential equations

$$\frac{dA}{dt} = \sum_{n=1}^{N} \epsilon^n \alpha_n + O(\epsilon^{N+1}) \qquad (3)$$

$$\frac{d\psi}{dt} = \omega_0 + \sum_{n=1}^{N} \epsilon^n \beta_n + O(\epsilon^{N+1}) \qquad (4)$$

The right hand side of Equations (3) and (4) are series expansions of ϵ, the gage function, and parameters α_n and β_n. These α_n and β_n terms are determined by integrating the nonlinear force term f(X) that appears in Equation (1) over the total period of the oscillation which is defined to be 2π. The amplitude

and phasing are thereby time dependent functions of the nonlinear load-displacement relationship defined by Equations (3) and (4).

In the asymptotic method, as in most perturbation methods, the linear system results are approached as ϵ approaches zero. In this case, the amplitude, A, becomes constant and the phasing, ψ, becomes a linear function of time with a constant frequency, Equations (3) and (4). The displacement in Equation (2) then takes the form of simple harmonic motion of linear elastic systems. The basis of the asymptotic solution approach is to determine the solutions of equations (2) through (4) for successively higher orders of ϵ. The procedure for determining the asymptotic solutions depend on deriving appropriate functional forms of U_n, α_n, and β_n. This is accomplished by expressing the load developed in the nonlinear root springs by

$$F(x) = K(x)X \tag{5}$$

K(X) is the nonlinear stiffness associated with the root support spring and X is the root displacement defined by Equation (2). To determine the U_n, α_n and β_n coefficients only the first term of Equation (5) is retained and this term is expanded in the Fourier Series. The functions α_n, β_n and U_n are expressed in terms of the coefficients of this Fourier Series and therefore are integrals of the nonlinear force term evaluated over a period of 2π. In this manner, the equations defining the asymptotic solutions of Equations (2) through (4) are completely defined. During this study the asymptotic solutions were obtained for first and second order approximations, i.e., terms in Equations (3) and (4) up to ϵ^2. The details of the Fourier Series expansions and the determination of the asymptotic solutions are given in Appendix B. The results of the asymptotic expansion for the two types of nonlinearities considered in this study are summarized below.

2.1 Freeplay Nonlinearity

The freeplay nonlinearity is illustrated in Figure 2(a). The asymptotic solution for the freeplay nonlinearity is derived directly from the equations

developed in the preceding section. The waveform of the developed load will take one of the two shapes shown in Figure 4, depending on the relationship between the magnitudes of the freeplay, S, and the amplitude, A, of displacement. For A less than S no load is developed, Figure 4(a). When A is greater than S the load is as shown in Figure 4(b). The nonlinear load is then determined by specifying the freeplay S and the amplitude A. The approach used throughout this study is based on derivation of the "effective" stiffness $\bar{K}$ of the nonlinear spring. This effective stiffness is used in Equation (5) to determine the corresponding load. With the effective load substituted in Equation (1), the equivalent linearized system is analyzed by conventional methods. It is the determination of this effective stiffness term that utilizes the asymptotic expansion techniques.

The "effective" stiffness $\bar{K}$ of the nonlinear spring including the influence of freeplay is defined in the asymptotic method as:

$$\bar{K} = K\left(1 + \varepsilon B_1 + \varepsilon^2 B_2 + \ldots \varepsilon^N B_N\right) \tag{6}$$

In this expression, the B_n terms are directly related to the β_n coefficients of the expansion of Equation (4). The relationship between the β_n and B_n terms is derived in Appendix B. Therefore, rather than actually solving Equation (4), once the β_n coefficients are determined and therefore the B_n's, the "effective" stiffness is computed from Equation (6) directly. For the freeplay nonlinearity all α_n coefficients are zero due to the symmetry of the freeplay nonlinearity and the single valued odd form of the nonlinear load. This implies, from Equation (3), that the amplitude of the limit cycle oscillation is constant.

The expression for the first order approximation of the effective stiffness, hereafter referred to as the first order solution, contains only the B_1 term in Equation (6). The form of this term (from Appendix B) is given as

$$\varepsilon B_1 = 0 \qquad (A<S)$$

$$\varepsilon B_1 = \frac{-1}{\pi}\left(1 - 2 t_1 + \cos t_1 \sin 2 t_1\right) \tag{7}$$

$$t_1 = \cos^{-1}\left(S/A\right) \tag{8}$$

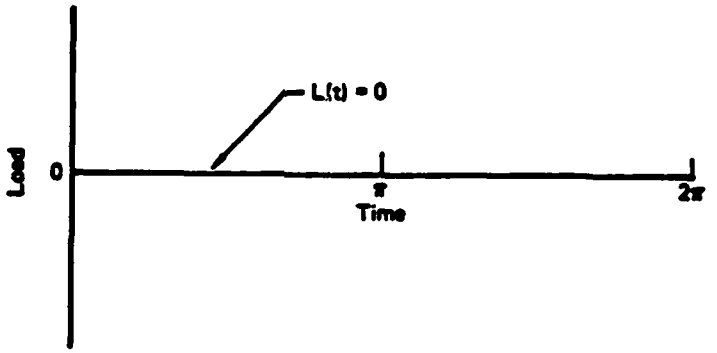

(a) Load (A<S)

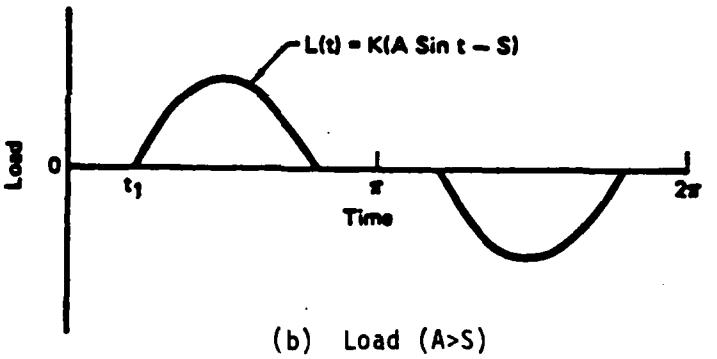

(b) Load (A>S)

FIGURE 4 DEVELOPED LOAD FOR FREEPLAY NONLINEARITY

Using Equations (6), (7) and (8) the relationship between the effective stiffness and the linear spring rate for a freeplay nonlinearity may be obtained to the first order.

The form of B_1 developed from the asymptotic expansion technique is identical to that developed using the describing-function, References 1 and 2. Since the describing function results, and hence the first order solutions are discussed in detail in References 1 through 4, they will only be summarized here for comparison and the remaining discussion focused on the higher order solutions.

The second order solution is obtained by adding the effect of second order terms to the first order solution. In order to determine the second order approximation of the effective stiffness, it is necessary to derive the expression for the B_2 coefficient that appears in Equation (6). Using the procedures for the asymptotic method, the second order correction term for a single degree of freedom with a freeplay nonlinearity is of the form (from Appendix B)

$$\varepsilon^2 B_2 = 0 \qquad (A<S)$$

$$\varepsilon^2 B_2 = -\frac{1}{\pi} \sum_{n=3,5}^{\infty} \frac{\Gamma_n}{n^2-1} \left[\Gamma_n - \frac{2}{n} \cos t_1 \sin nt_1\right] \tag{9}$$

where

$$\Gamma_n = \left[\frac{\sin (n-1)t_1}{2(n-1)} + \frac{\sin (n+1)t_1}{2(n+1)}\right] \tag{10}$$

and t_1 is definded in Equation (8). The second order correction terms of Equation (9) contains the coefficients of the fundamental harmonic in the Fourier Series expansion of the load and coefficients of all higher order harmonics. Therefore the second order solutions are not restricted, as is the describing-function approach of References 1 through 4, to a one-term, first harmonic approximation. Substituting Equations (7) through (10) into Equation (6), the relationship between the effective stiffness and the linear spring rate for a freeplay nonlinearity may be obtained for the second order approximation. This relationship is shown in Figure 5 as a function of the amplitude of motion to freeplay ratio, (A/S). For amplitude ratios (A/S) less than 1, the effective stiffness is zero. As the amplitude increases, the magnitude of K approaches that of linear stiffness K. This corresponds physically to the nonlinearity becoming less and less significant as the (A/S) ratio increases and ϵ approaching zero in Equations (3) and (4).

As shown in Figure 5, there is little difference in the results of the first and second order solutions where the nonlinearity is most significant, low (A/S) values, and the solutions converge very rapidly as (A/S) increases. The implication here is that the stiffness behavior of system with a freeplay nonlinearity is dominated almost completely by the fundamental harmonic and the second order corrections have little impact on the response. For a single degree of freedom system, the effective stiffness value can be expressed in terms of an effective frequency of the nonlinear system. For the stiffness ratios shown in Figure 5, the corresponding first and second order solutions expressed in terms of frequency are shown in Figure 6. In this figure the asymptotic solutions are compared with numerical simulation results obtained for a single degree of freedom system in Reference 1. As the figure indicates, the asymptotic solutions predict frequency ratios very close to those given by the numerical simulation.

2.2 Preload Nonlinearity

For the preload nonlinearity shown in Figure 2(b), the asymptotic functions or displacements, defined by Equation 2, were modified to account for the non-symmetry of the load displacement relationship. This displacement func-

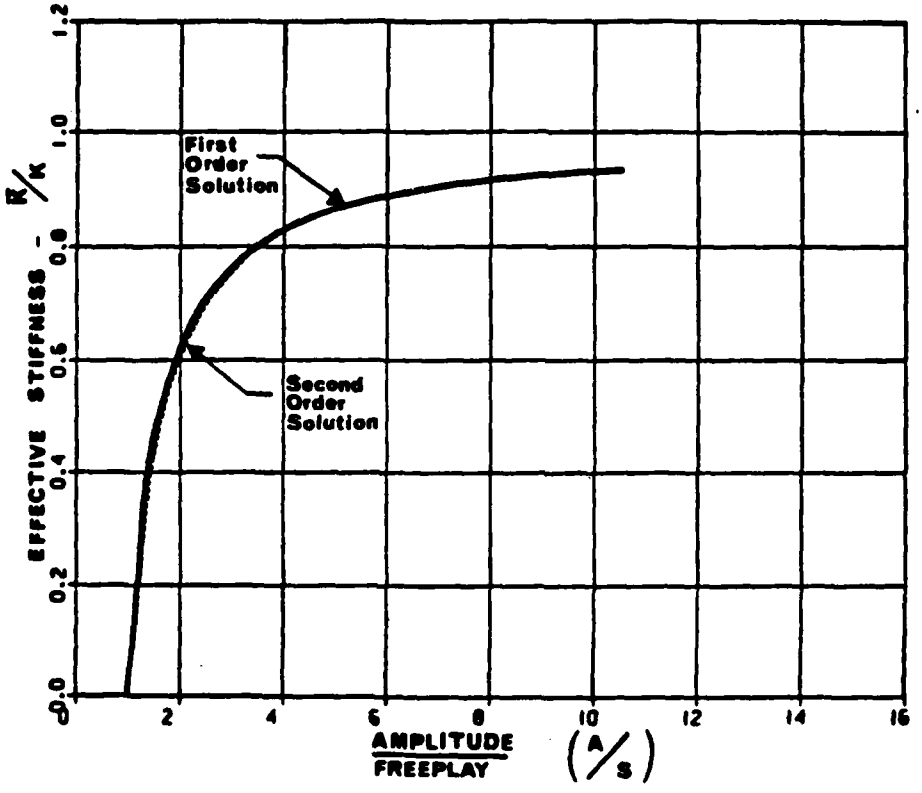

FIGURE 5 EFFECTIVE STIFFNESS RATIO FOR A FREEPLAY NONLINEARITY

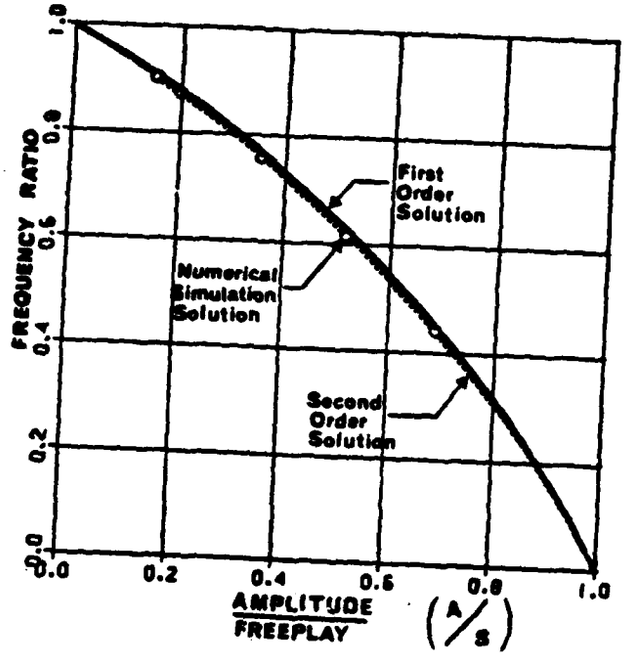

FIGURE 6 COMPARISON OF ASYMPTOTIC AND NUMERICAL SIMULATION RESULTS FOR A FREEPLAY NONLINEARITY

tion was assumed to be of a similar form to that used in Reference 1 and is

$$X = A_0 + A_1 \cos \psi + \sum_{n=1}^{N} \varepsilon^n U_n (A,\psi) + O(\varepsilon^{N+1}) \qquad (11)$$

The coefficients A_0 and A_1 were defined such that the energy stored in the nonlinear spring is the same for both positive and negative displacements. In addition, it was required that Equation (11) result in a positive amplitude equal to the initial displacement. Thus, the amplitude coefficients that appear in Equation (11) are obtained from

$$A_1 = \frac{A}{2} + \frac{1}{2}\sqrt{2PA - P^2} \qquad (P \leq A \leq P+2S) \qquad (12)$$

$$A_1 = \frac{A}{2} + \frac{1}{2}\sqrt{(A-2S)^2 + 4PS} \qquad (A > P+2S) \qquad (13)$$

In both cases, the coefficient A_0 is obtained from the relationship

$$A = A_1 + A_0 \qquad (14)$$

It has been assumed that the influence of a preload nonlinearity is related to positive displacements of the system. When amplitude of motion, A, is less than the preload P, A_1 equals A and A_0 is zero. For this situation, the nonlinear problem is reduced to a linear problem.

The waveform of the developed load in the nonlinear spring will take the shapes shown in Figure 7. As before, these waveforms are dependent on the relationship between the magnitudes of the freeplay, preload and amplitude of motion. Proceeding as was done for the freeplay case, the coefficients of Equation (6) were defined using the load displacement relationship illustrated in Figure 7. The first order approximation to the "effective" stiffness is of the form

$$\varepsilon B_1 = 1.0 \qquad (A<P) \qquad (15)$$

$$\varepsilon B_1 = \frac{1}{\pi}\left[\pi - t_1 + \frac{2}{A_1}(P-A_0)\sin t_1 - \frac{1}{2}\sin 2t_1\right] \qquad (16)$$

$$(P<A<P+2S)$$

For amplitude of motion $A \geq P+2S$ we have,

$$\varepsilon B_1 = \frac{1}{\pi}\left[\pi + t_1 - t_2 - \frac{2}{A_1}(P+2S-A_0)\sin t_1 + \right. \qquad (17)$$

$$\left. \frac{2}{A_1}(P-A_0)\sin t_2 + \frac{1}{2}(\sin 2t_1 - \sin 2t_2)\right]$$

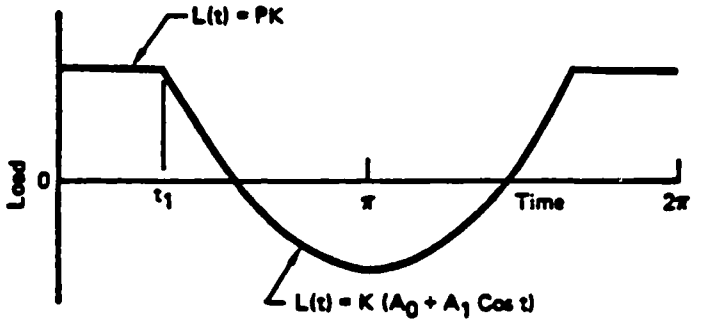

(a) LOAD (A>P+2S)

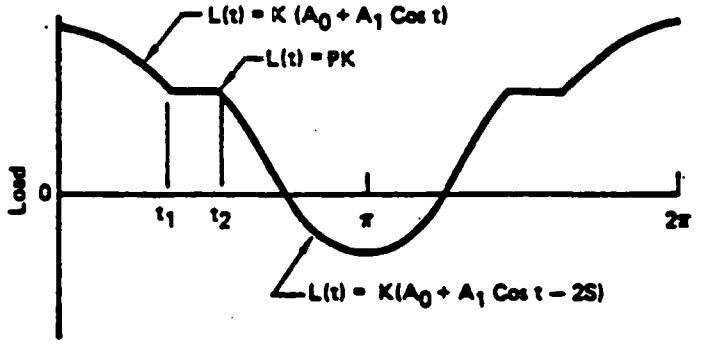

(b) LOAD (A>P+2S)

FIGURE 7 DEVELOPED LOAD FOR PRELOAD NONLINEARITY

where $$t_1 = \cos^{-1}\left(\frac{P-A_o}{A_1}\right) \tag{18}$$

$$t_2 = \cos^{-1}\left(\frac{P+2S - A_o}{A_1}\right) \tag{19}$$

As was determined for the freeplay case the first order asymptotic solution and the describing-function solution of References 1 and 2 are equivalent. Proceeding to the second order approximation the B_2 coefficient of Equation (6) is of the form (from Appendix B)

$$\varepsilon^2 B_2 = -\frac{1}{\pi}\sum_{n=2}^{\infty}\frac{\Gamma_n}{n^2-1}\left\{\frac{1}{n\pi}\left[2(P-A_o)\sin nt_1 - \Gamma_n\right]\right\} \tag{20}$$

Γ_n is defined by Equation (10), t_1 by Equation (16) and B_1 is given by Equation (15). For the amplitudes $A \geq P+2S$

$$\varepsilon^2 B_2 = -\frac{1}{\pi}\sum_{n=2}^{\infty}\frac{\sigma_n}{n^2-1}\left\{\frac{1}{n\pi}\left[\left(\frac{A_o-P}{A_1}\right)\left(\sin nt_1 - \sin nt_2\right)\right]\right. \tag{21}$$

$$\left. -\left(2\cos t_1 \sin nt_1\right) + \sigma_n\right\}$$

B_1 and t_2 are defined by Equations (17) and (19) and

$$\sigma_n = \left[\frac{\sin (n-1)t_2 - \sin (n-1)t_1}{2(n-1)} + \frac{\sin (n+1)t_2 - \sin (n+1)t_1}{2(n+1)}\right] \tag{22}$$

The first and second order solutions for the stiffness ratio is plotted in Figure 8 as a function of the amplitude of motion to freeplay ratio for a freeplay to preload ratio (S/P) of one. For amplitudes of motion less than the preload P the frequency ratio is one and the response is linear. As the amplitudes of motion increases, the stiffness, and in turn, the frequency decreases. This softening response is due to the deadspace in the spring causing the effective stiffness to be less than the linear value. As the amplitude increases well beyond the nonlinear region, the influence of the nonlinearity becomes small and the magnitude of frequency coefficient approaches one.

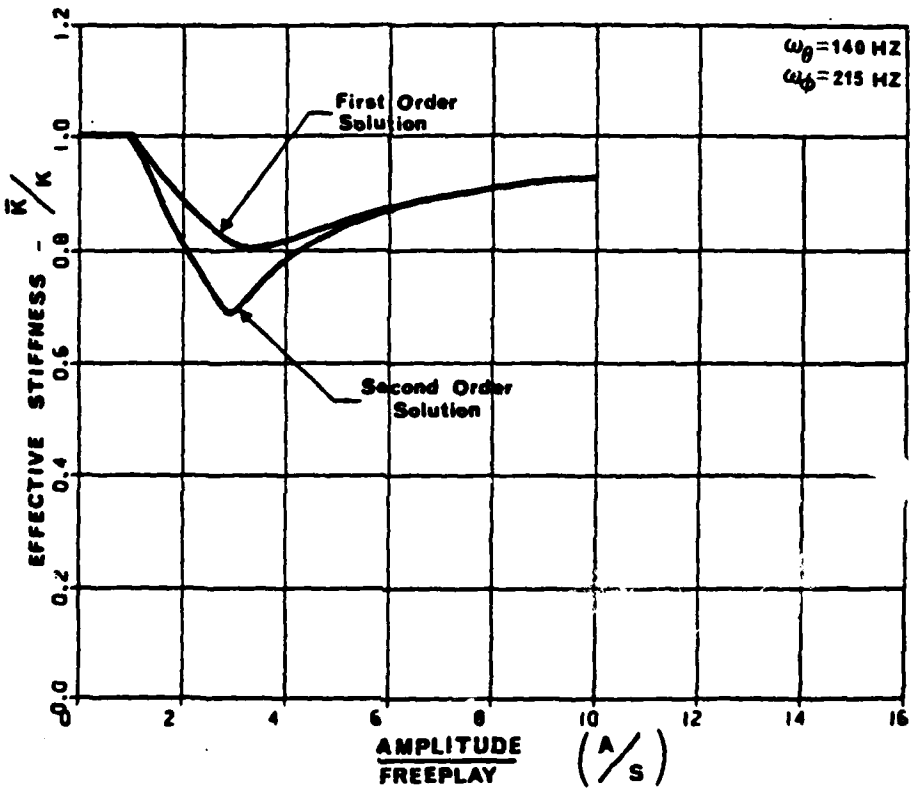

FIGURE 8 EFFECTIVE STIFFNESS RATIO FOR A PRELOAD NONLINEARITY

While both first and second order solutions shown in Figure 8 exhibit the same trends, the second order solution predicts a significantly greater reduction in stiffness for amplitudes of motion near P+2S where the nonlinearity is most significant. At higher values of the amplitude, the first and second order solutions converge and asymptotically approach the linear solution. The difference in the two solutions near the nonlinear region is directly a result of including higher harmonics in the second order approximation. These harmonics are seen to influence the response most when the amplitudes of motion fall within the deadband region of the load displacement curve, Figure 7.

A comparison between the asymptotic solutions and numerical solutions are shown in Figure 9. The numerical solutions, Reference 1, were obtained by directly integrating the single degree of freedom equations of motion. Figure 9 shows that the first order approximation (describing-function) is unconservative in predicting the effective frequency behavior when compared to the numerical results for amplitudes near the preload-plus-freeplay region, (A/S=3). On the other hand, the second order solution tends to be conservative in predicting the effective stiffness. At amplitudes of motion near or greater than twice the preload-plus-freplay values, there is little difference between the numerical and first or second order solutions. Based on these comparisons, it is apparent that the higher harmonics contribute significantly to the response at amplitudes of motion near the nonlinear region of the load-displacement relationship for the preload nonlinearity.

2.3 Time History Results

In addition to the computation of the effective stiffness of the nonlinear system, the asymptotic method provides a means of obtaining higher order approximations to the response time history. The time dependent motion of the nonlinear system as defined in the asymptotic method is given by Equation (2). In this expression, the functions U_n contain the contributions of higher harmonics in the response and exclude any contribution of the fundamental harmonic. Application of the asymptotic method consists of determining the appropriate expression for U_n based on the order of the asymptotic approximation and the number of harmonics desired. The general form for the expression for each type of nonlinearity considered in this study is given below.

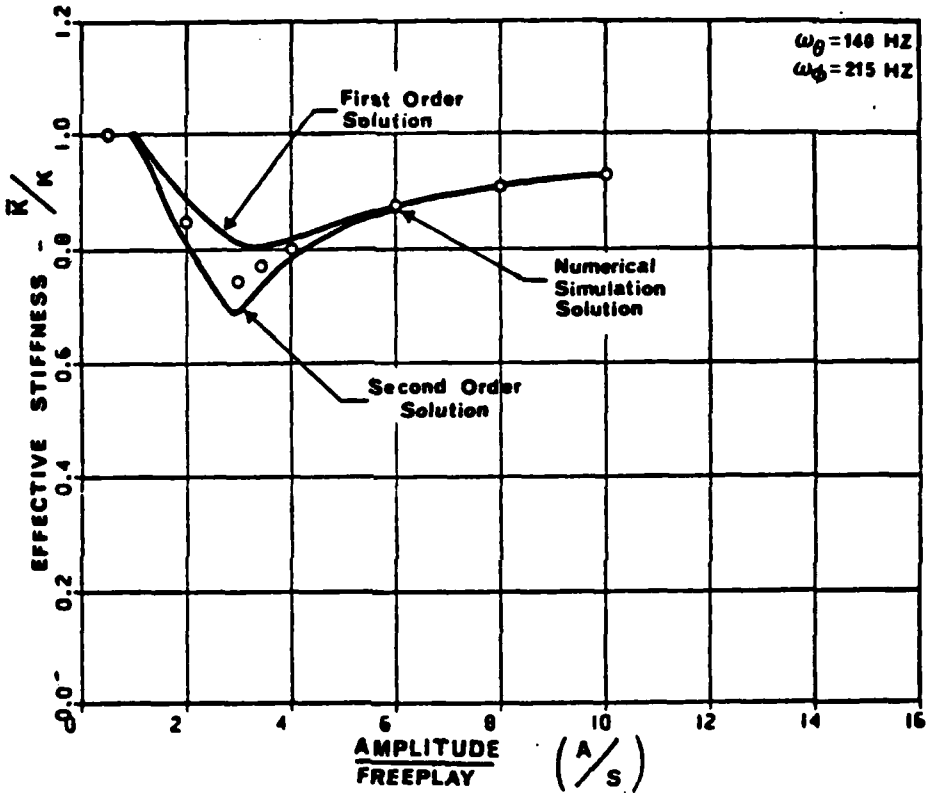

FIGURE 9 COMPARISON OF ASYMPTOTIC AND NUMERICAL SIMULATION RESULTS FOR A PRELOAD NONLINEARITY

2.3.1 Freeplay Nonlinearity

For the freeplay nonlinearity the form of the U function is determined using the coefficients of the Fourier Series expansion of the load displacement relationship. From the results of Appendix B to the second order

$$U_1 = -\frac{1}{\pi}\sum_{n=3,5}^{\infty}\left[\Gamma_n - \frac{2}{n}\cos t_1 \sin nt_1\right]\cos n\bar{\omega}t \qquad (23)$$

N is odd, Γ_n is defined in Equation (10) and $\bar{\omega}$ is the effective frequency.

The time history results for the freeplay nonlinearity are shown in Figures 10 and 11. In Figure 10, the time history response, defined by Equation (2), is plotted for an A/S ratio of 3 and an initial amplitude of 0.2^{o}. The limit cycle motion shown in Figure 10 exhibits a very regular periodic motion with an almost constant amplitude and frequency corresponding to effective stiffness value determined by the relationship defined in Paragraph 2.1. The period of the time history indicates that the response is controlled almost entirely by the fundamental harmonic, the first term of Equation (2). The time history of the second term of Equation (2), corresponding to the contribution of higher harmonics, is shown in Figure 11. Terms up to the eleventh harmonic were included in Equation (23) in the determination of U. Note that although the frequency of U is higher, the amplitude is significantly lower than that of fundamental harmonic. These results are consistent with the comparisons between the first and second order solutions discussed in Paragraph 2.1. The results show the first order solution utilizing a one term Fourier Series expansion of the load is sufficient for the freeplay nonlinearity and the higher harmonics of the second order solutions have little impact on the system response.

2.3.2 Preload Nonlinearity

For the preload nonlinearity the form of the U function is determined in the same manner as was done for the freeplay case. From the results of Appendix B the second order solutions for amplitudes of motion in the range $P \leq A \leq P+2S$ is defined as

$$U_1 = -\frac{1}{\pi}\left[2\left(\frac{P}{A_1}\right)t_1 + (2\pi - t_1)\frac{A_o}{A_1} - 2\sin t_1\right] - \frac{1}{\pi}\sum_{n=2}^{\infty}\frac{\cos n\bar{\omega}t}{n^2-1}\left\{\frac{1}{n\pi}\left[(P-A_o)\sin nt_1 - \Gamma_n\right]\right\} \qquad (24)$$

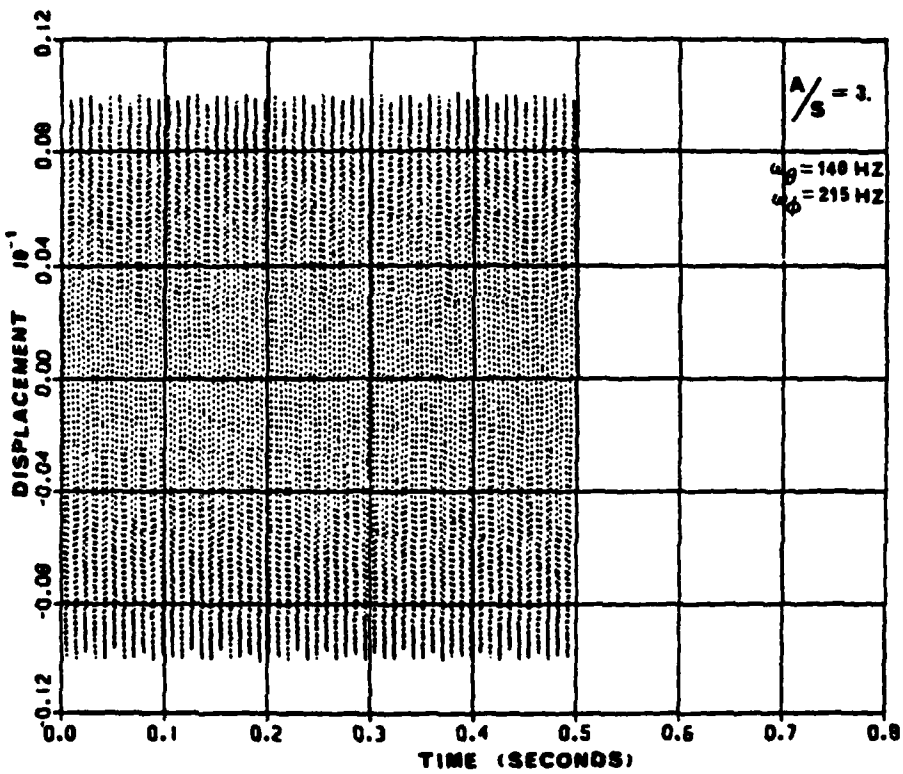

FIGURE 10 LIMIT CYCLE TIME HISTORY: FUNDAMENTAL PLUS HIGHER HARMONICS - FREEPLAY NONLINEARITY

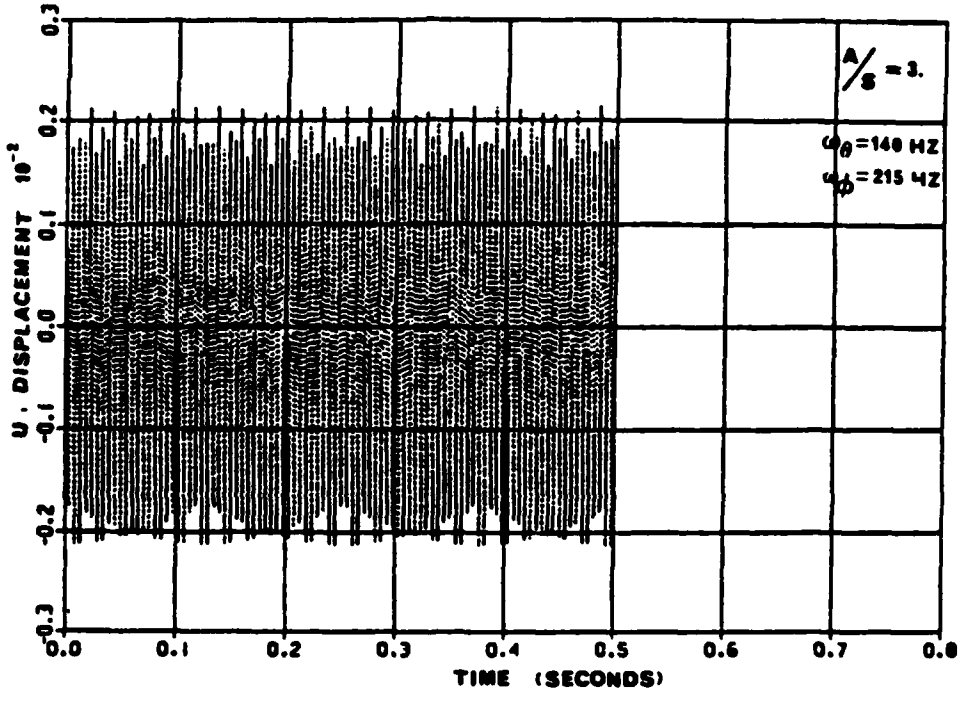

FIGURE 11 TIME HISTORY: HIGHER HARMONIC - FREEPLAY NONLINEARITY

Γ_n and t_1 are given in Equations (10) and (16). For amplitudes of motion $A \geq P+2S$

$$U_1 = \frac{1}{\pi}\left[\frac{A_o}{A_1}\left(t_1 + \pi - t_2\right) + \left(\sin t_1 - \sin t_2\right) + \frac{P}{A_1}\left(t_2 - t_1\right) - 2\left(\frac{S}{A_1}\right) t_1\right] - \frac{1}{\pi}\sum_{n=2}^{\infty} \frac{\cos n\bar{\omega}t}{n^2-1}\left\{\frac{1}{n\pi}\left[\left(\frac{A_o-P}{A_1}\right)\left(\sin nt_1 - \sin nt_2\right)\right] - 2\cos t_1 \sin nt_1 + \sigma_n\right\} \tag{25}$$

t_1, t_2 and σ_n are defined by Equations (18), (19) and (22).

The time history results for the preload cases are shown in Figures 12 and 13. In Figure 12 the displacement time history for a preload nonlinearity with an initial amplitude of 0.2^o is shown. In this figure the two distinguishing features of the preload time history is the offset of the response from zero and the presence of higher harmonics in the response. The offset is due to the presence of the preload and the unsymmetric nature of the nonlinear load-displacement relationship. The higher harmonics in the amplitude are due to the contribution of terms appearing in U. The time history plot of the higher harmonics in the U coefficient is shown in Figure 13. In Figure 13 the offset in the response is also present. Also note that comparing the magnitude of the time histories in Figures 12 and 13 shows that the U terms are greater than forty percent of the total amplitude. This indicates that a significant amount of the strain energy developed in the root support springs cycles with a frequency greater than the frequency of the fundamental harmonic. Based on these observations, the influence of higher harmonics is seen to be significant in the prediction of both the effective frequency and limit cycle response of the system response for a preload nonlinearity.

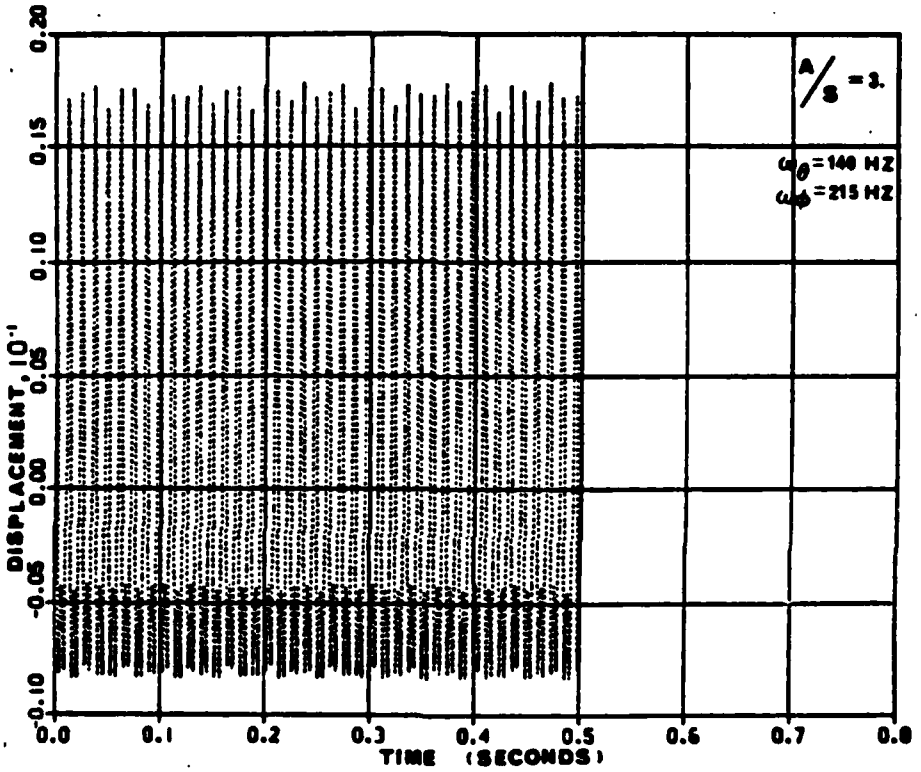

FIGURE 12 LIMIT CYCLE TIME HISTORY: FUNDAMENTAL PLUS HIGHER HARMONICS - PRELOAD NONLINEARITY

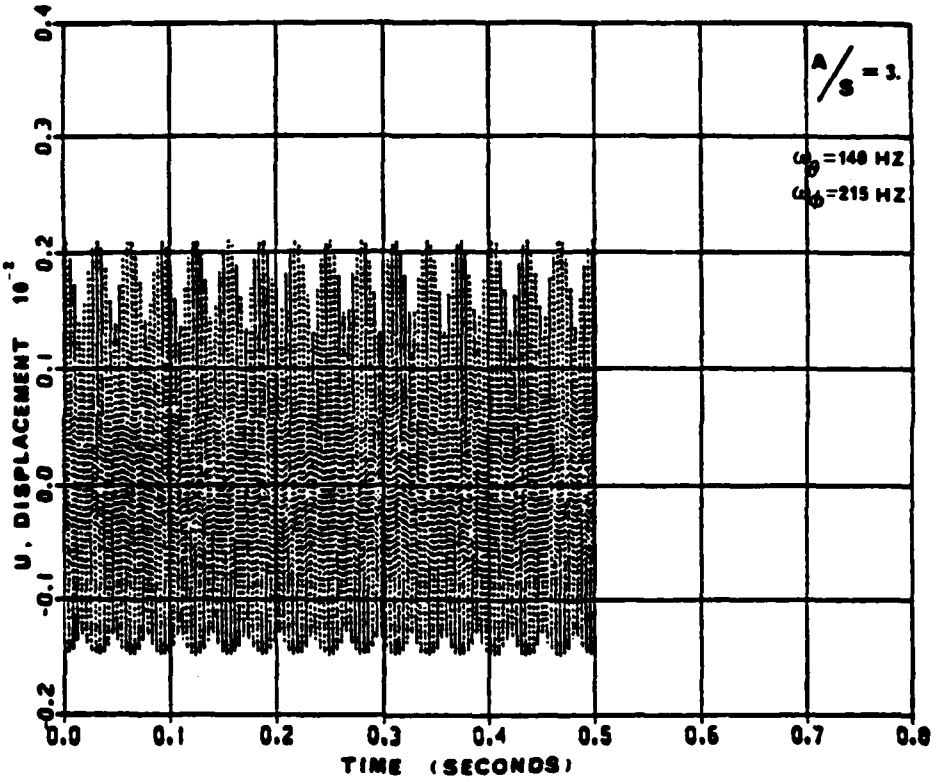

FIGURE 13 TIME HISTORY: HIGHER HARMONIC - PRELOAD NONLINEARITY

3.0 DETERMINATION OF AERODYNAMIC SURFACE LIMIT CYCLE RESPONSE

In this section the equations and techniques developed in Section 2.0 for the freeplay and preload nonlinearities are applied to predict the limit cycle response of the baseline aerodynamic surface. The frequency and dynamic pressure at which the limit cycle oscillations are sustained were determined as a function of the amplitude of motion and magnitude of the nonlinearity. The aeroelastic data used was based on linear flutter results obtained for the effective system where the nonlinear terms in the equations of motion were replaced by the corresponding effective stiffness calculated by the asymptotic methods. The flutter results for both a rigid and flexible representation of the baseline aerodynamic surface were determined using standard eigenanalysis procedures and are presented in Appendix A.

The geometry and physical characteristics of the baseline control surface are also presented in Appendix A. The results of this section and Appendix A are for a specific aerodynamic surface using a simplified aerodynamic theory. However, the application of the developed procedure is not restricted to these conditions. The procedures are applicable to a variety of surface geometries, aerodynamic theories or flutter analysis techniques.

Application of the asymptotic expansion results to predict the limit cycle response of the baseline aerodynamic surface follows the same procedure as developed in References 1 and 2. The effective uncoupled frequency was calculated from the asymptotic solutions for each nonlinearity and corresponding degree of freedom. The dynamic pressure defined by Equation 26, at which the limit cycle oscillation is sustained, was then determined from the data in Appendix A.

$$q = \frac{1}{2} \rho U^2 \tag{26}$$

The results for the freeplay and preload nonlinearities considered in this study follow.

3.1 FREEPLAY NONLINEARITY

The procedure followed to determine the limit cycle response of the aerodynamic surface with root freeplay structural nonlinearities is shown in Figure 14. This figure shows the step-by-step procedure for introducing the nonlinear effects in either or both root pitch and root roll degrees of freedom.

Results for the rigid baseline control surface with a freeplay nonlinearity in the root pitch degree of freedom are shown in Figure 15. These results are for a freeplay nonlinearity in the root pitch degree of freedom, S_β, of 0.2 degrees and an uncoupled root pitch frequency of $215H_z$. The data indicates the variation in the effective dynamic pressure at which limit cycle oscillations will be sustained as a function of the amplitude-to-freeplay ratios in the root pitch degree of freedom. This figure shows the influence of the freeplay nonlinearity is most pronounced for amplitudes of motion near the freeplay value. For successively larger amplitudes of motion, the effective stiffness approaches the uncoupled stiffness value and the critical dynamic pressure approaches that of the linear system.

The results obtained using the first and second order asymptotic solutions to predict the limit cycle behavior are compared in Figure 15. They indicate, as was found in Section 2.0, that the first and second order solutions differ only slightly for the freeplay case. Again, this behavior is attributed to the dominance of the fundamental harmonic in the response.

Results for freeplay nonlinearities in root roll and for two freeplay nonlinearities were found to differ only slightly from those of References 1 and 2. The results for these cases are not repeated here and the reader is referred to References 1 and 2 for more details on the influence of freeplay nonlinearities on the limit cycle behavior.

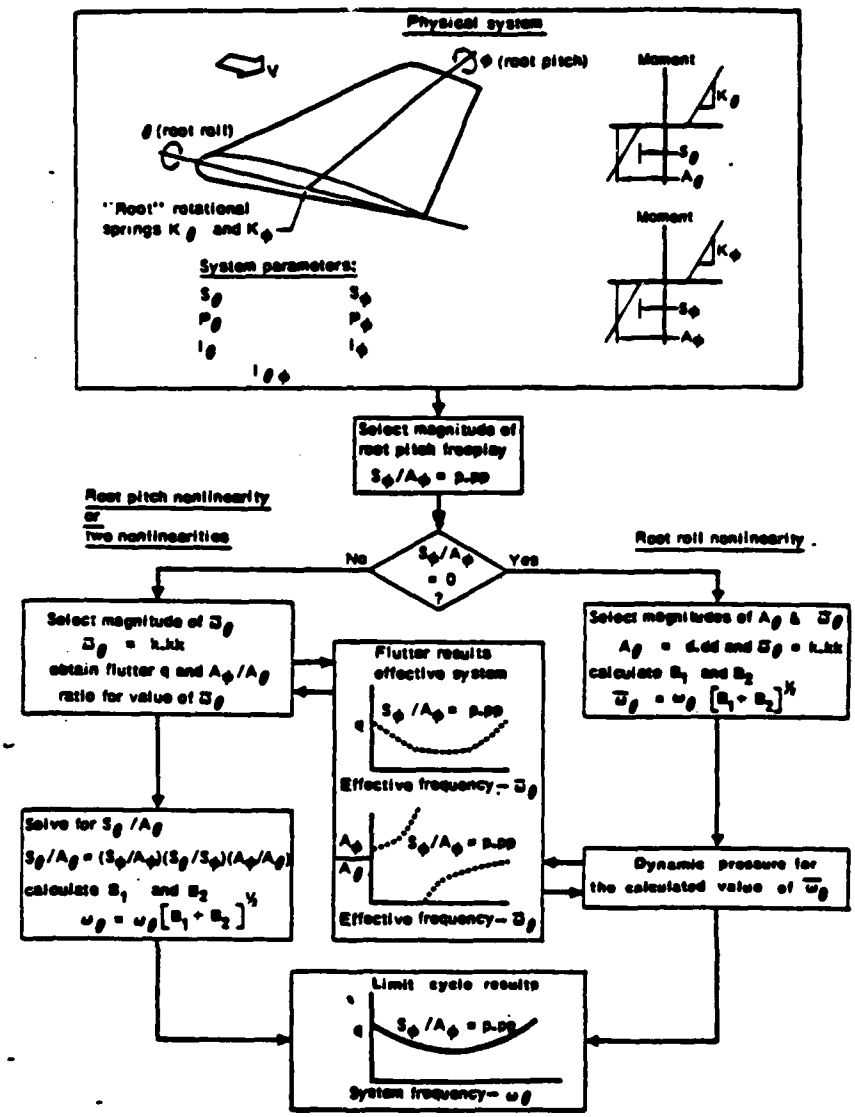

FIGURE 14 COMPUTATIONAL PROCEDURE FOR A FREEPLAY NONLINEARITY

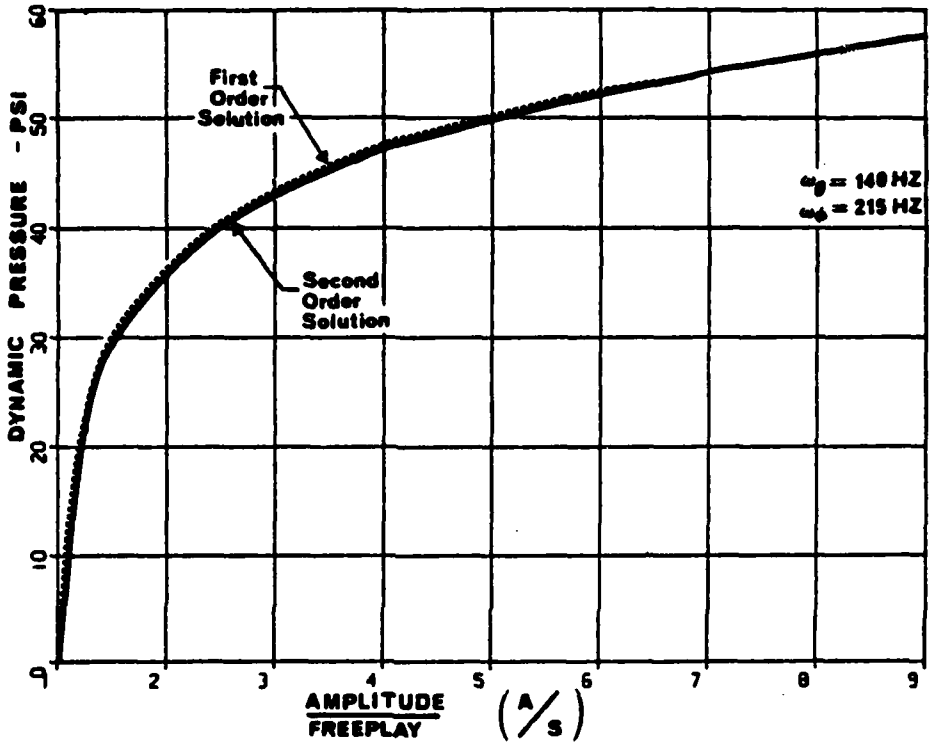

FIGURE 15 DYNAMIC PRESSURE TO SUSTAIN LIMIT CYCLE OSCILLATION; RIGID SURFACE WITH ROOT PITCH FREEPLAY NONLINEARITY

3.2 PRELOAD NONLINEARITY

The procedure used for predicting the limit cycle response of the rigid baseline control surface with a preload nonlinearity is very similar to that presented in the preceding section for the freeplay nonlinearity. The computational steps to be followed to predict the limit cycle response are shown in Figure 16. Linear system flutter analyses are conducted for variations in the effective stiffness parameter. These flutter results are then modified to account for the presence of the structural nonlinearities.

Using the second order asymptotic solutions, the results shown in Figure 17 were obtained for a rigid control surface having a single root roll preload nonlinearity. This figure shows the change in the dynamic pressure as a function of root roll amplitude of motion to freeplay ratio, A/S, for varying freeplay-to-preload, S/P, ratios. For amplitudes of motion less than the preload, the critical dynamic pressure equals the flutter dynamic pressure of the linear system. As the amplitude of motion increases, the influence of the freeplay is reflected in the rise of the dynamic pressure. This occurs as a result of the softening effect on the effective root roll stiffness which results in a higher dynamic pressure for this particular aerodynamic surface. As the amplitude of motion continues to increase, the influence of the nonlinearity decreases and the results again approach those of the linear system.

In Figure 18 the results obtained for both first and second order asymptotic solutions are shown for a preload nonlinearity in the root pitch degree of freedom for a rigid control surface. From this figure the influence of the higher harmonics is apparent. While the trends are basically the same, the second order solution predicts a lower value of critical dynamic pressure to sustain the limit cycle oscillation than does the first order solution for amplitudes of motion near the P+2S value. This is directly related to the effective stiffness behavior predicted for this amplitude range as was discussed in Section 2.0 and illustrated in Figure 8.

First and second order solutions for the rigid baseline control surface having preload nonlinearities in both root degrees of freedom are shown in

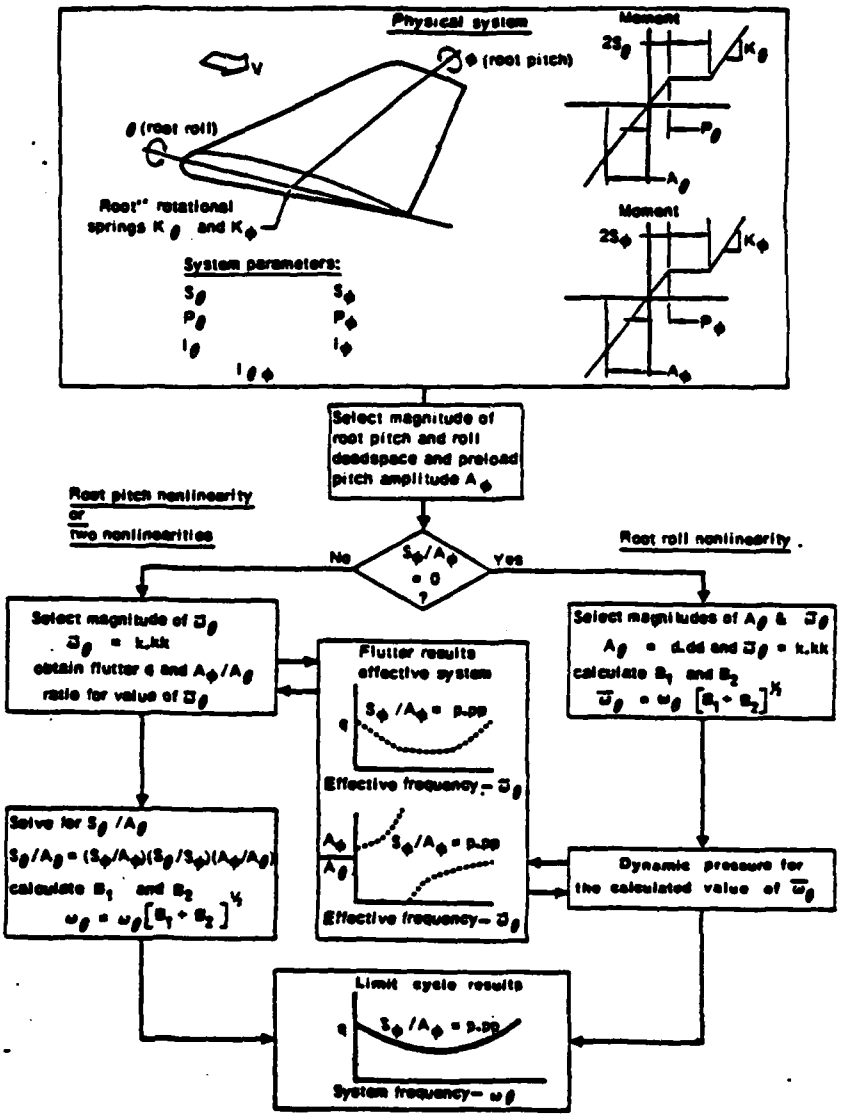

FIGURE 16 COMPUTATIONAL PROCEDURE FOR A PRELOAD NONLINEARITY

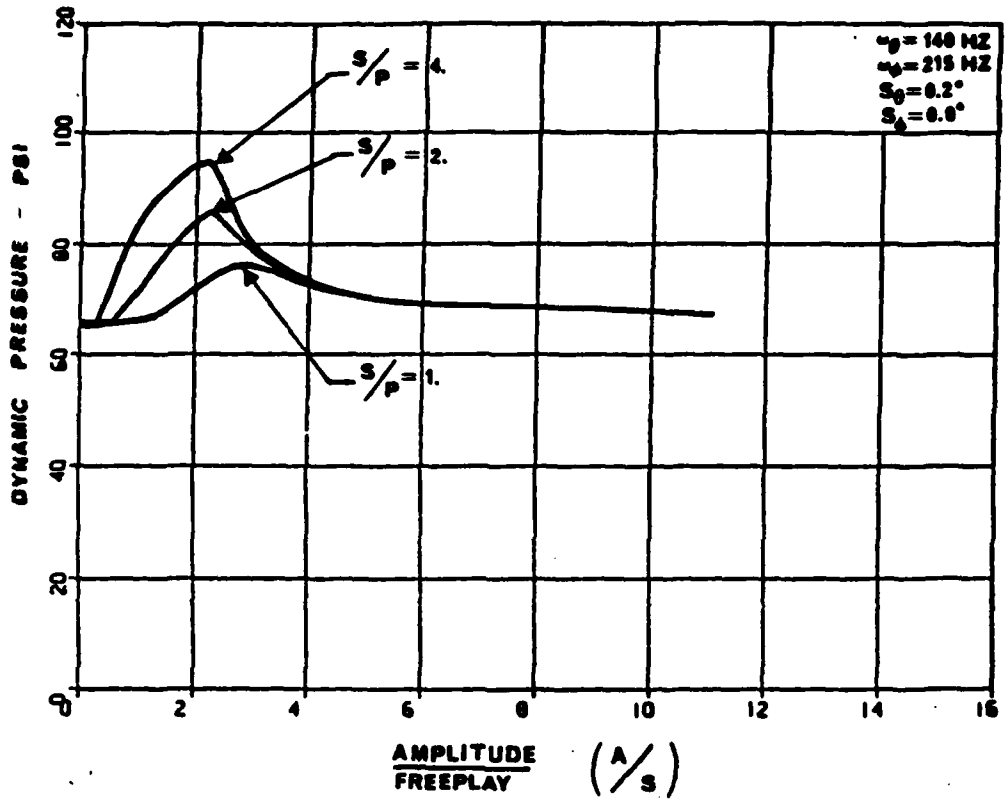

FIGURE 17 DYNAMIC PRESSURE TO SUSTAIN LIMIT CYCLE OSCILLATION; RIGID SURFACE WITH ROOT ROLL PRELOAD NONLINEARITY

Figure 19. The results presented are for a 0.2 degree freeplay region in both degrees of freedom and a freeplay-to-preload, S/P, ratio of two. The two pair of curves shown in this figure are for two different values of the amplitude-to-freeplay ratio, S/A. The effective stiffness of the preload nonlinearity is a double-valued function as illustrated in Figure 8. Therefore, the results shown in Figure 19 are for double-valued amplitude of motion ratios. The larger S/A values correspond to amplitudes less than the quantity P+2S, whereas the lower ratios correspond to amplitudes in excess of this value.

As for the case of a single nonlinearity, the presence of the higher harmonics can substantially change the prediction of the limit cycle response. In both Figures 18 and 19, the nonlinearity in root pitch is more critical in terms of initiating a limit cycle response. For root pitch nonlinearities the results indicate that the limit cycle response amplitude can be several times greater than the magnitude of the freeplay and can be sustained at dynamic pressures well below the flutter critical value.

A flexible control surface having a preload nonlinearities in both root degrees of freedom was also studied. The results for a 0.2 degree freeplay in both root degrees of freedom and a freeplay-to-preload ratio, S/P, of two are shown in Figure 20. As with the rigid control surface studies of Figures 18 and 19, the amplitude ratios are double valued.

Figure 20 shows that at higher uncoupled roll frequencies, the second order solutions predict a somewhat higher critical dynamic pressure than does the first order solution at the same amplitude-to-freeplay ratio. This behavior is a direct result of the linear flutter data, as the trends in the effective stiffness are the same for both the rigid and flexible cases.

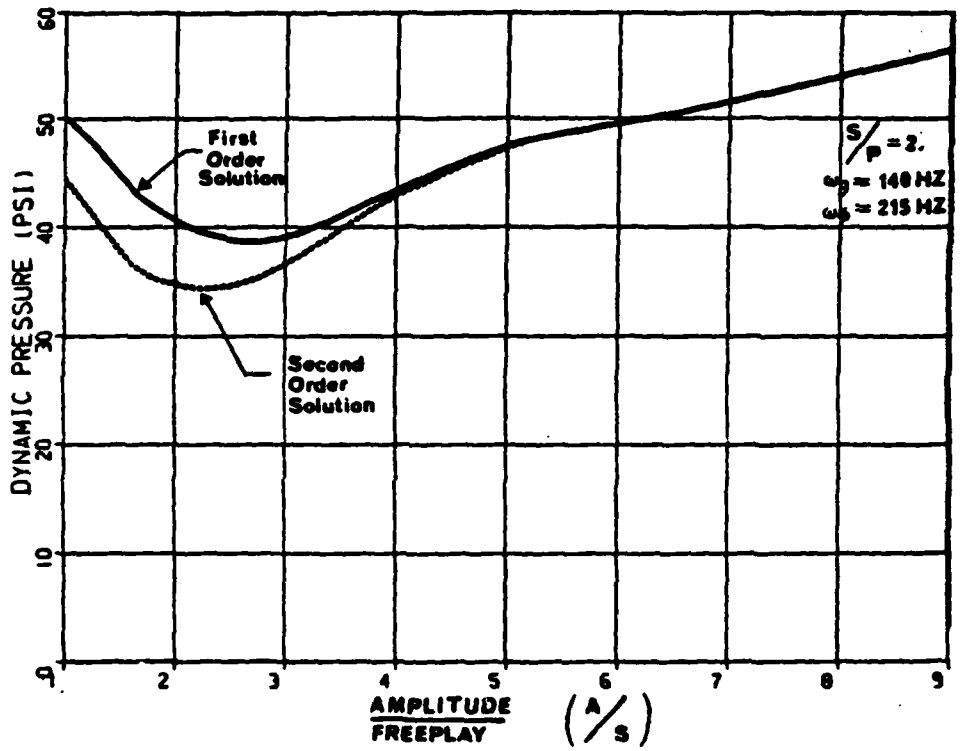

FIGURE 18 DYNAMIC PRESSURE TO SUSTAIN LIMIT CYCLE OSCILLATION; RIGID SURFACE WITH ROOT PITCH PRELOAD NONLINEARITY

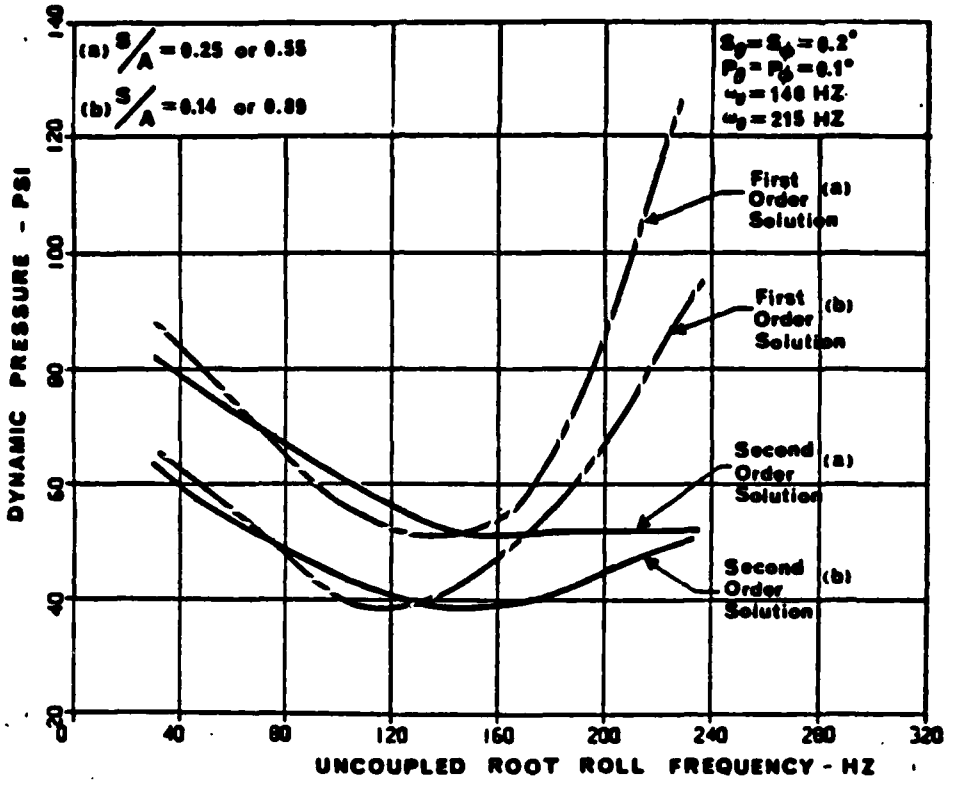

FIGURE 19 DYNAMIC PRESSURE TO SUSTAIN LIMIT CYCLE OSCILLATION; RIGID SURFACE WITH PRELOAD NONLINEARITIES IN ROOT PITCH AND ROLL

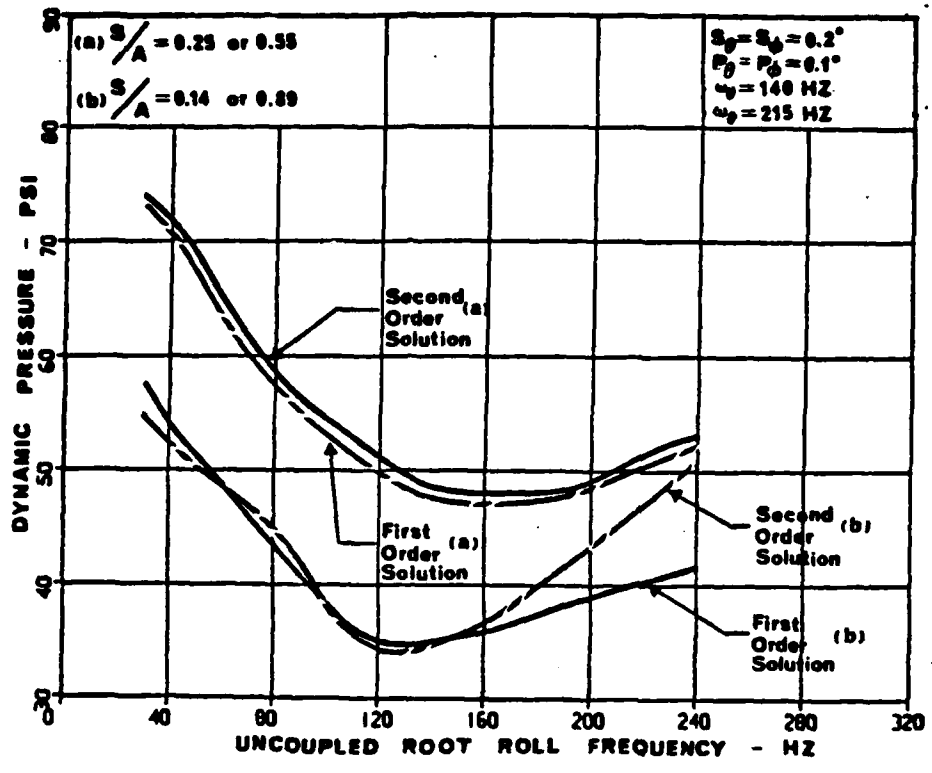

FIGURE 20 DYNAMIC PRESSURE TO SUSTAIN LIMIT CYCLE OSCILLATION; FLEXIBLE SURFACE WITH PRELOAD NONLINEARITIES IN ROOT PITCH AND ROLL

3.3 CORRELATION WITH NUMERICAL RESULTS

The asymptotic solutions obtained in the preceding paragraph were briefly compared with the numerical simulation results of Reference 1. The objective here was to compare the results of the describing-function (first order) solutions and the asymptotic (second order) solutions with the "exact" numerical solutions in the accuracy critical regions. From the results of Reference 1 it was concluded that the worst correlation between the describing-function results and simulation results was observed for the case of a flexible control surface with two preload nonlinearities. The authors of Reference 1 attributed this discrepency to the influence of higher harmonics neglected in the describing-function approach. For this reason this configuration was used to compare the three solution approaches.

The aeroelastic response results for the flexible baseline control surface with two preload nonlinearities is shown in Figure 21. The dynamic pressure required to sustain the limit cycle oscillation is plotted as a function of the freeplay-to-amplitude ratio, S/A. The curves are for a system with uncoupled pitch and roll frequencies of 215Hz and 140 Hz, respectively. In Figure 21(a), the root roll motion is shown, and in Figure 22(b) the root pitch motion is shown. The results of these comparisons show a better correlation between the second order asymptotic solution and the numerical simulations than was obtained using the first order solutions. This supports the conclusions of Reference 1 that the source of the error in the one term describing-function approach is a result of the higher harmonics not being included in modeling the nonlinear behavior.

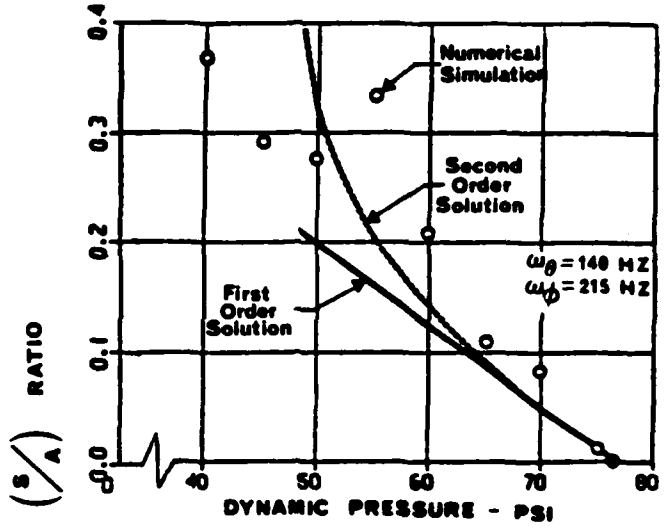

(a) Root Roll Motion

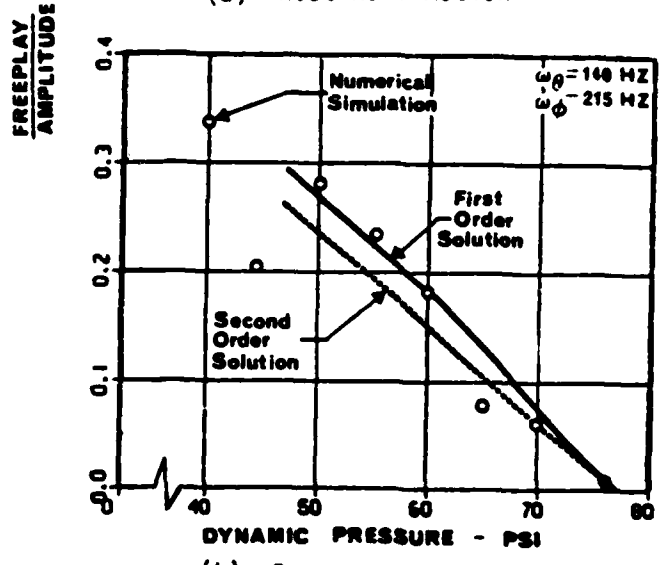

(b) Root Pitch Motion

FIGURE 21 COMPARISON OF PREDICTED AND SIMULATION RESULTS FOR A FLEXIBLE CONTROL SURFACE WITH A PRELOAD NONLINEARITY IN PITCH AND ROLL

4.0 CONCLUSION

The presence of structural nonlinearities can adversely affect the aeroelastic response of aerodynamic surfaces. Of particular concern is the occurance of a sustained limit cycle response which may lead to structural damage of the aerodynamic surface, support structure and equipment components such as control actuators. The results obtained during this study show that aerodynamic surfaces with structural nonlinearities can become susceptible to limit cycle behavior at dynamic pressures below the linear flutter value. The nature of the limit cycle response was found to be a constant amplitude motion with a steady state frequency expressed as a function of the magnitude of the nonlinearity and the amplitude of the oscillation.

The objective of the present study was to develop an analysis procedure to predict aerosurface limit cycle response that retains the flexibility and well defined procedures of the describing-function approach, yet provides greater accuracy and generality in modeling the nonlinear system behavior. This was accomplished by using an asymptotic expansion technique to derive a relationship between the parameters characterizing the structural nonlinearity and the amplitude and frequency of the limit cycle response.

The overall conclusion from this investigation is that the use of the asymptotic expansion method results in an accurate prediction of the aerodynamic surface limit cycle response. The procedure described in this study was used to investigate the interrelationship between the magnitude of the nonlinearities, flight conditions and the nature of the resulting limit cycle response. First and second order asymptotic solutions were developed for a freeplay type nonlinearity with and without a linear preload in the root support structure. The asymptotic solutions, which contain the contribution of higher harmonics, were compared with the describing-function approach which contains only the first harmonic. It was shown that the first order asymptotic solutions and the describing-function approach were identical and the higher order asymptotic solutions could be used to account for the contribution of higher harmonics in the limit cycle response.

The significance of the higher harmonics in predicting the nature of the limit cycle response was found to depend on the particular nonlinearity studied. During the development of the second order asymptotic solutions for the freeplay nonlinearity it was concluded that the higher harmonics had small effect on the results. Even for amplitudes near the freeplay magnitudes, where the nonlinear effect is strongest, the higher harmonics were found to have little influence. These results are reasonable when one considers the exceptionally good correlation demonstrated between the first order, single term solution and the exact numerical solution. It is concluded that little is gained in the prediction of limit cycle response by including the higher order solutions for the freeplay nonlinearity.

In the case of the preload nonlinearity the influence of higher harmonics was found to have a definite impact on the predicted limit cycle response. When the first and second order solutions were compared for this nonlinearity, the latter predicted a considerably greater reduction in the effective stiffness at amplitudes near the freeplay region of the load-displacement curve. This behavior was observed to be consistent with the numerical simulation results presented in Reference 1. As the amplitude of motion became larger than the preload-plus-freeplay magnitude, the first and second order asymptotic approximations of the effective stiffness converged. As amplitudes increased further both solutions approach the linear solution results. In addition to the influence on the effective stiffness values the higher harmonics were also seen to contribute to the form of the expressions to determine the limit cycle time history response. Variations of amplitude in the computed waveform for the limit cycle response could be attributed directly to these higher order harmonics. It was concluded from these results that for the preload type nonlinearity the second order asymptotic solutions should be used to accurately predict the nature of the limit cycle response.

This study has shown the applicability of the asymptotic expansion approach to account for the influence of structural nonlinearities in the limit cycle response analysis of aerodynamic surfaces. The method developed employs the asymptotic solutions to determine the effective system parameters governing the

nonlinear response. The ability to include the influence of higher harmonics in the nonlinear load-displacement relationship and obtain solution accuracies to any desired order have been demonstrated. The methods were applied to two simple nonlinear systems and the potential influence of higher order solutions on the limit cycle response was investigated. The applicability of the asymptotic methods, however, is not restricted to these nonlinearities or undamped systems. Investigations of the asymptotic solutions for systems with other types of nonlinearities, including nonlinear damping dependent on the displacement and/or its derivatives, are feasible using this approach.

5.0 REFERENCES

1. Laurenson, R. M., and Trn, R. M., "Flutter of Control Surfaces with Structural Nonlinearities," AIAA Journal, Volume 18, Number 10, 1979, pp. 1245-1251.

2. Briley, R. P. and Laurenson, R. M., "Flutter of Control Surfaces with Structural Nonlinearities, Phase II," Final Report, MDC E2354, McDonnell Douglas Astronautics Company - St. Louis Division, May 1980, (N00019-76-C-606).

3. Woolston, D. S., Runyan, H. L., and Andrews, R. E., "An Investigation of Effects of Certain Types of Structural Nonlinearities on Wing and Control Surface Flutter," Journal of the Aeronautical Sciences, January 1957, pp. 57-63.

4. Shen, S. F., "An Approximate Analysis of Nonlinear Flutter Problems," Journal of the Aerospace Sciences, January 1959, pp. 25-32, 45.

5. McIntosh, S. C., Reed, R. E., and Rodeen, W. P., "An Experimental and Theoretical Study of Nonlinear Flutter," Final Report for NAVAIR Contract N00019-78-C-0118, NEAR TR 209, October 1979.

6. Bogolivbov, N. N., Mitropolsky, Y. A., Asymptotic Methods in the Theory of Non-Linear Oscillations, Hindustan Publishing Co., DELHI, 1961.

7. Nayfeh, A. H., Perturbation Methods, Wiley, New York, 1973.

8. Desmarais, R. N. and Reed, W. H., "Wing/Store Flutter with Nonlinear Pylon Stiffness," AIAA/ASME/ASCE/AHS Structural Dynamics and Material Conference, Seattle, WA, 12-14 May 1980, Paper 80-0792.

LIST OF SYMBOLS

A	Amplitude of motion at surface root support
a_i	Fourier series coefficient
B_1, B_2	Stiffness correction terms derived from asymptotic expansions
b_i	Fourier series coefficients
F(x)	Nonlinear load term in root spring
g_n	Fourier series coefficients
h_n	Fourier series coefficients
I	Rigid control surface inertia properties
K	Linear spring rate of root springs
K	Effective spring rate of root springs
M	System mass
N	Order of asymptotic expansion
$O(\epsilon^N)$	Higher order terms of order N
P	Nonlinear preload value
Q	Aerodynamic forcing function
S	Nonlinear freeplay value
t	Time
U_N	Asymptotic expansion functions
αN	Asymptotic expansion coefficients
βN	Asymptotic expansion coefficient
ϵ^N	Gage function
ϕ	Displacement in root pitch
	Displacement in root roll
	Uncoupled natural frequency of linearized system
	Phasing function

Subscripts

n	General indicies
ϕ	Associated with root pitch degree of freedom
θ	Associated with root roll degree of freedom

APPENDIX A
Flutter Analysis of Baseline Aerodynamic Surface

The aeroelastic analysis performed in this study utilized the flutter results for the effective or linearized representation of the baseline aerodynamic surface. The physical description of the baseline surface and the flutter results for both rigid and flexible cases are discussed below.

Properties of the Harpoon missile control surface were used to define the baseline surface configuration which was used throughout the study. The geometric configuration of the control surface is shown in Figure A-1. The structural nonlinearities that were investigated are associated with the root support. Presented in Figure A-2 are the inertia properties of the control surface. The first two rows and the columns of the inertia matrix are associated with rigid root roll and pitch motions while the last two diagonal elements are the generalized masses of the control surface modes. The off-diagonal terms, the PF quantities, represent the inertia coupling between rigid and flexible motions. The mode shapes associated with the first two control surface cantilever modes are given in Figure A-3. These modal data were used when investigating a flexible control surface configuration.

Representative flutter results for the baseline control surface take the form illustrated in Figures A-4 and A-5. The results given in Figure A-4 are for a rigid fin while those for the flexible fin are given in Figure A-5. These two figures show the variation in the flutter critical dynamic pressure as a function of the effective root roll frequency for various values of the effective root roll frequency.

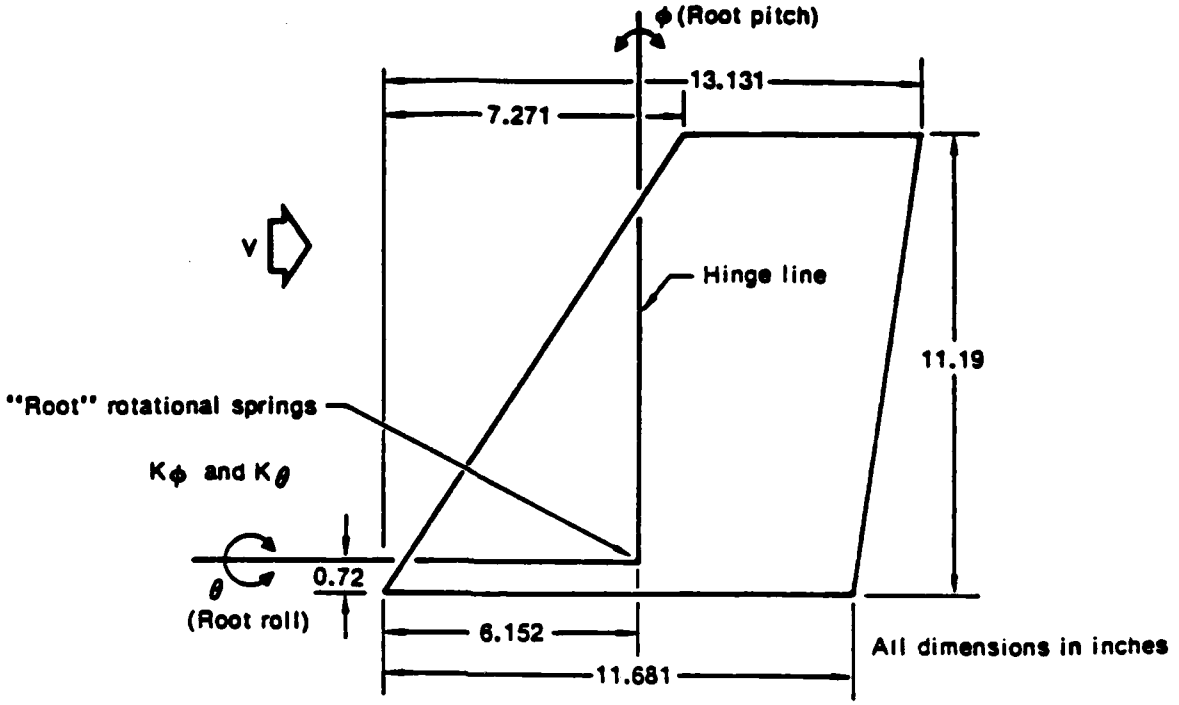

Figure A-1 Control surface geometry

$$\begin{bmatrix} I_\theta & I_{\theta\phi} & PF_{\theta 1} & PF_{\theta 2} \\ & I_\phi & PF_{\phi 1} & PF_{\phi 2} \\ & & m_1 & 0 \\ \text{Symmetric} & & & m_2 \end{bmatrix}$$

(a) Form of inertia matrix

$I_\theta = 0.1667$ lb-sec^2-in. $\quad PF_{\theta 1} = -7.227 \times 10^{-3}$ lb-sec^2

$I_\phi = 0.071$ lb-sec^2-in. $\quad PF_{\theta 2} = -1.014 \times 10^{-3}$ lb-sec^2

$I_{\theta\phi} = 0.058$ lb-sec^2-in. $\quad PF_{\phi 2} = -3.212 \times 10^{-3}$ lb-sec^2

$m_1 = 4.220 \times 10^{-4}$ lb-sec^2/in. $\quad PF_{\phi 2} = 2.134 \times 10^{-3}$ lb-sec^2

$m_2 = 4.295 \times 10^{-4}$ lb-sec^2/in.

(b) Specific inertia terms

Figure A-2 Control surface inertia properties

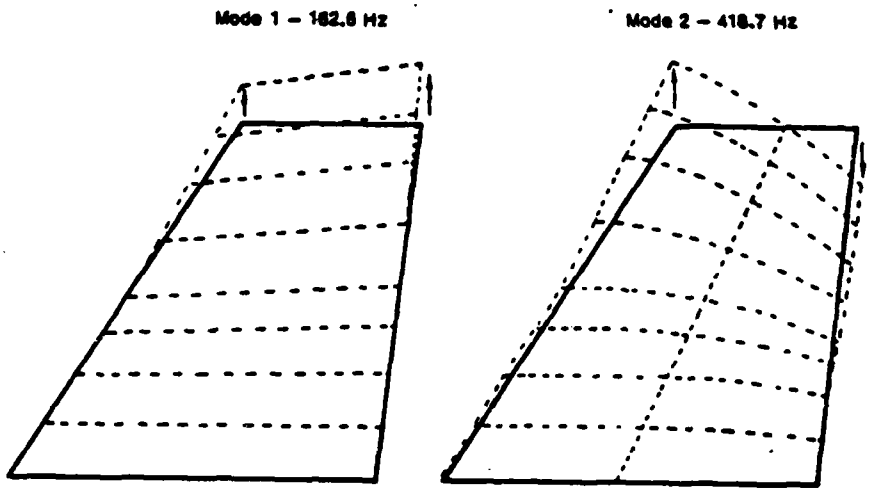

FIGURE A-3 CONTROL SURFACE CANTILEVER MODES

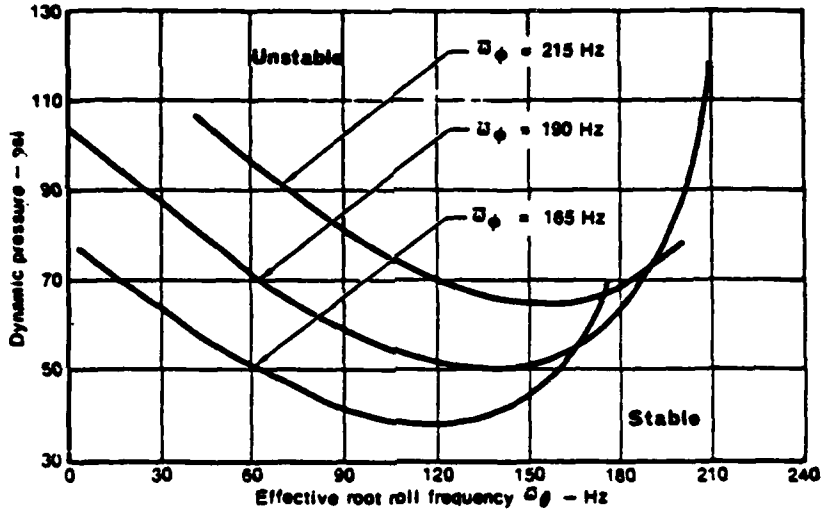

(a) DYNAMIC PRESSURE

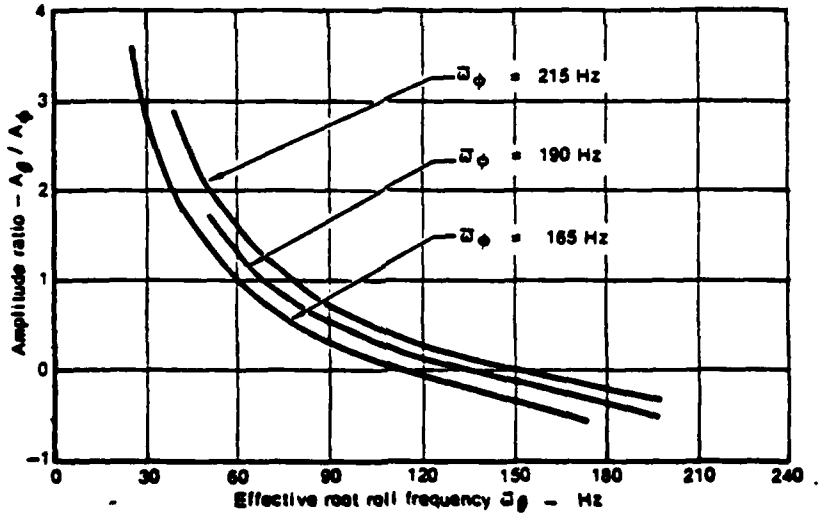

(b) AMPLITUDE RATIO

FIGURE A-4 EFFECTIVE SYSTEM RIGID CONTROL SURFACE FLUTTER RESULTS

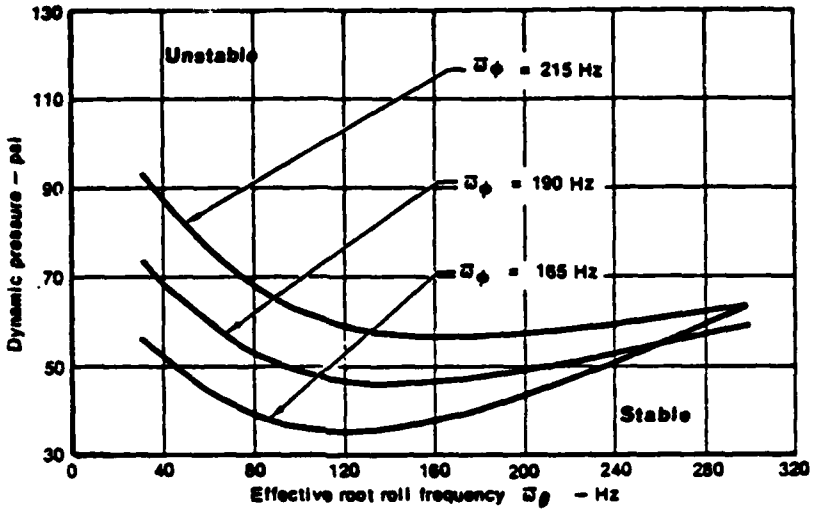

(a) DYNAMIC PRESSURE

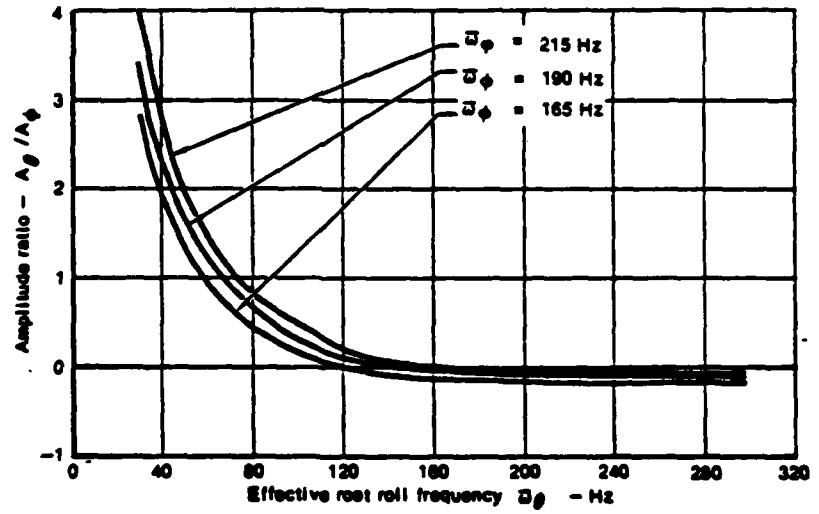

(b) AMPLITUDE RATIO

FIGURE A-5 EFFECTIVE SYSTEM FLEXIBLE CONTROL SURFACE FLUTTER RESULTS

APPENDIX B
DETAILED DEVELOPMENT OF THE ASYMPTOTIC SOLUTIONS

In the discussions of the asymptotic solutions presented in Section 2.0, the first and second order approximations to the limit cycle response were presented. The details of the computational steps are given here for the freeplay and preload nonlinearities.

As discussed in Section 2.0 the nonlinear equations of motion for the system considered in this study can be written as

$$\frac{d^2x}{dt^2} + \omega_o{}^2 x = \varepsilon f(x) + Q(x) \tag{B1}$$

In the asymptotic expansion methods, the solution of Equation (B1) is assumed to be of the form

$$x = A \cos \psi + \sum_{n=1}^{N} \varepsilon^n U_n (A,\psi) + O(\varepsilon^{N+1}) \tag{B2}$$

The amplitude A, and phasing parameter ψ are determined from

$$\frac{dA}{dt} = \sum_{n=1}^{N} \varepsilon^n \alpha_n + O(\varepsilon^{N+1}) \tag{B3}$$

$$\frac{d\psi}{dt} = \omega_o + \sum_{n=1}^{N} \varepsilon^n \beta_n + O(\varepsilon^{N+1}) \tag{B4}$$

The term N indicates the order of the asymptotic approximation. For this study solutions up to the second order (N=2) were determined. The β_n and B_n terms of Equations (B3) and (B1) are functions that satisfy Equation (B1) and are expressed in terms of coefficients obtained from the Fourier Series expansion of the nonlinear function f(X) in Equation (B1).

*In Appendix B, the number in the second bracket identifies identical equations from Section 2.0. As equations (B-1), (B-2), (B-3) and (B-4) were discussed in detail in Section 2.0 they will just be presented here. Refer to Section 2.0 for a complete description of these equations.

The first step in the solution procedure is to determine functions α_1, α_2, β_1, β_2, and U_1. These functions can be derived by expanding the nonlinear function f (ψ) in a Fourier Series, substituting Equations B2 through B4 into Equation B1 and equating coefficients of sin ψ and cos ψ. These functions are given by the following relations,

$$\alpha_1 = -\frac{1}{2\pi\omega_o}\int_o^{2\pi} f\ (A\cos\psi)\sin\psi d\psi \tag{B5}$$

$$\beta_1 = -\frac{1}{2\pi\omega\ A}\int_o^{2\pi} f\ (A\cos\psi)\cos\psi d\psi \tag{B6}$$

$$U_1 = \frac{g_o}{\omega_o^2} - \frac{1}{\omega_o^2}\sum_{n=2}^{\infty}\frac{g_n\cos n\psi + h_n\sin n\psi}{n^2-1} \tag{B7}$$

where

$$g_n = \frac{1}{2\pi}\int_o^{2\pi} f\ (A\cos\psi)\cos n\psi d\psi \tag{B8}$$

$$h_n = \frac{1}{2\pi}\int_o^{2\pi} f\ (A\cos\psi)\sin n\psi d\psi \tag{B9}$$

The terms α_1, β_1, g_n and h_n are the coefficients of the Fourier Series expansion of the nonlinear force f(X) acting on the system. The second order coefficients α_2 and β_2 can be expressed in terms of Equations (B5) through (B7) and the derivative of f(X) as

$$\alpha_2 = \frac{-1}{2\omega}\left\{2\,\alpha_1\,\beta_1 + \alpha_1\,A\,\frac{d_{\beta 1}}{dA}\right\} - \frac{1}{2\pi\omega}\int_o^{2\pi}\overline{\Phi}\sin\psi d\psi \tag{B10}$$

$$\beta_2 = \frac{1}{2\omega}\left\{\beta_1^{\,2} - \frac{\alpha_1}{A}\frac{d\alpha_1}{dA} - \frac{1}{2\pi\omega_o A}\right\}\int_o^{2\pi}\overline{\Phi}\cos\psi d\psi \tag{B11}$$

$$\overline{\Phi} = \left[U_1\,f_x'\left(A\cos\psi\right) + \left(\alpha_1\cos\psi - A\beta_1\sin\psi + \omega\frac{\partial U_1}{\partial\psi}\right)f_x''\right] \tag{B12}$$

By computing the terms in Equations (B5) through (B12), substituting into Equations (B3) and (B4) and integrating, the amplitude A and phasing parameter, ψ approximated to the second order, are obtained.

Equations (B5) through (B12) are for the general case. For the two nonlinearities considered in this study, these equations can be reduced to a much simpler form. First, the form of f(X) for the freeplay and preload nonlinearities is such that all α_n and h_n terms in Equations (B5), (B10), and (B9) are identically zero. For this case, Equations (B3) and (B4) yield

$$A = \text{const} \tag{B13}$$

$$\psi = \bar{\omega}t = \left(\omega_o + \varepsilon\beta_1 + \varepsilon^2 \beta_2\right)t + \text{const.} \tag{B14}$$

$$\text{or} \quad \bar{\omega} = \left(\omega_o + \varepsilon\beta_1 + \varepsilon^2 \beta_2\right) \tag{B15}$$

where $\bar{\omega}$ is the effective frequency approximated to the second order. Equations (B7) and (B1) then become

$$U_1 = \frac{g_o(\alpha)}{\omega_o^2} - \frac{1}{\omega_o^2} \sum_{n=2}^{\infty} \frac{g_n \cos \psi}{n^2-1} \tag{B16}$$

$$\beta_2 = -\frac{\beta_1^2}{2\omega} - \frac{1}{2\pi\omega_o A} \int_o^{2\pi} \bar{\Phi} \cos \psi d\psi \tag{B17}$$

The computational effort of this study was centered on determining U_1, β_1 and β_2 given by Equations (B6), (B16) and (B17), respectively.

The form of the effective stiffness to the second order given by Equation (4) is

$$\bar{K} = K\left(1 + \varepsilon B_1 + \varepsilon^2 B_2 + \ldots \varepsilon^N B_N\right) \tag{B18}$$

This expression can be obtained from Equation (B15) by squaring both sides and retaining term up to ϵ^2. This yields,

$$\bar{\omega}^2 = \omega_o^2 \left[1 + \frac{2\epsilon}{\omega_o} \beta_1 + \frac{\epsilon^2}{\omega_o^2} \left(\beta_1^2 + 2\beta_2 \omega_o\right)\right] \tag{B19}$$

Substituting Equations (B6) and (B17) for β_1 and β_2 into Equation (B19) and simplifying yields

$$\bar{\omega}^2 = \omega_o \left[1 + \epsilon B_1 + \epsilon^2 B_2\right] \tag{B20}$$

The relationship between B_1 and B_2 and β_1 is defined as

$$B_1 = 2 \frac{\beta_1}{\omega_o} \tag{B21}$$

$$B_1 = \frac{1^o}{\pi A \omega_o^2} \int_o^{2\pi} f\ (A \cos \psi) \cos \psi d\psi \tag{B22}$$

where Φ is defined by equation B-12.
Note that here it is implied that

$$B_2 = -\frac{1}{\pi \omega_o^2 A} \int_o^{2\pi} \Phi \cos \psi d\psi \tag{B23}$$

$$\lim_{\epsilon \to o} \bar{\omega}^2 = \omega_o^2 \tag{B24}$$

Using the relationship between the effective stiffness and natural frequency, Equation (B18) is obtained directly from (B20).

Summarizing the computational procedure, the first step is to compute $_o$ for the linear system. Then the term β_1 is obtained from Equation (B6). Next coefficients B_1 and B_2 can be determined using Equations (B12), (B21) and (B22). At this point the second order correction to the effective stiffness is obtained from Equation (B18). The computation of the time domain solution then requires solution of Equations (B8), (B14) and (B16). The form of these relationships are presented below for the two nonlinearities considered in this study.

FREEPLAY NONLLINEARITY

In order to compute the coefficients of the asymptotic approximations, the initial step is to expand the load relationships, L(t) in a Fourier Series. This load relationship is shown in Figure 4 of the text and is expressed as

$$L(t) = \begin{cases} 0 & \text{for } 0 < t < t_1 \\ K[A \sin t - S] & \text{for } t_1 < t < 2\pi \end{cases} \tag{B25}$$

This load is in the form of the function $F(A\cos\psi)$ in Equation (B21) so the first Fourier coefficient corresponds to the B_1 term in Equation (B20). Since the load function L(t) is a single-valued odd function its Fourier Series representation is of the form

$$L(t) = \sum_{n=1}^{\infty} b_n \cos n t \tag{B26}$$

$$b_n = \frac{1}{2\pi} \int_0^{2\pi} L(t) \cos n t \tag{B27}$$

As mentioned above the b_1 term of Equation (B27) and B_1 in Equation (B20) are related by the expression

$$B_1 = -\left(\frac{1}{A\omega_o^2} b_1 - 1\right) \tag{B28}$$

The form of the b_1 term for the load of Equation (B25) is,

$$b_1 = \frac{A\omega_o^2}{2\pi} \left(\pi - 2 t_1 - \sin 2 t_1\right) \tag{B29}$$

Computation of the B_2 term of Equation (B23) requires the coefficients of the higher harmonics of Equation (B26). A general expression for these higher harmonics is determined as

$$b_n = 0 \qquad (n = 2,4,\ldots) \tag{B30}$$

$$b_n = \frac{\omega_o A}{\pi} \left[\Gamma_N - \frac{S}{n} \sin n t_1\right] \qquad (n = 1,3,5\ldots) \tag{B31}$$

$$\Gamma_n = \left[\frac{\sin (n-1)t_1}{2(n-1)} + \frac{\sin (n+1)t_1}{2(n+1)}\right] \tag{B32}$$

By successive substitution of Equation (B30) into Equations (B16), (B12) and (B23) the B_2 coefficient of Equation (B18) is obtained. The form for the freeplay nonlinearity is given in Equation (B33).

$$B_2 = -\frac{1}{\pi} \sum_{n=3.5}^{\infty} \frac{\Gamma_n}{n^2-1} \left[\Gamma_n - \frac{2}{n} \cos t_1 \sin nt_1\right] \tag{B33}$$

PRELOAD NONLINEARITY

The procedure for deriving the coefficients of the asymptotic approximation of Equation (B18) for the preload nonlinearity follows the same procedure used for the freeplay nonlinearity. The load-displacement relation for the preload nonlinearity is shown in Figure 7 and is defined as

$$L(t) = \begin{cases} (A_0 + A_1 \cos t - 2S)K & \text{for } 0 < t < t_1 \\ PK & \text{for } t_1 < t < t_2 \\ (A_0 + A_1 \cos t)K & \text{for } t_2 < t < 2\pi - t_2 \\ PK & \text{for } 2\pi - t_2 < t < 2\pi - t_1 \\ (A_0 + A_1 \cos t - 2S)K & \text{for } 2\pi - t_1 < t < 2\pi \end{cases} \tag{B34}$$

where

$$t_1 = \cos^{-1}\left(\frac{P + 2S - A_0}{A_1}\right) \tag{B35}$$

$$t_2 = \cos^{-1}\left(\frac{P - A_0}{A_1}\right) \tag{B36}$$

The Fourier Series expansion of the load relationship is defined as

$$L(t) = \frac{b_0}{2} + \sum_{n=1}^{\infty} b_n \cos nt + \alpha_n \sin nt \tag{B37}$$

$$b_0 = \frac{1}{2\pi} \int_0^{2\pi} L(t)\, dt \tag{B38}$$

b_n is given by Equation (B27) and all α_n coefficients are zero for the function given by Equation (B34).

The b_n coefficients of Equation (B35) for the preload nonlinearity where $P < A \leq P+2S$ are

$$b_o = \frac{\omega_o^2 A_1}{\pi}\left[2 A_o \left(\pi - t_1\right) + 2 P t_1 - 2 A_1 \sin t_1\right] \tag{B39}$$

$$b_1 = \frac{\omega_o^2 A_1}{\pi}\left[\pi - t_1 + \frac{2}{A_1}\left(P - A_o\right) \sin t_1 - \frac{1}{2} \sin 2 t_1\right] \tag{B40}$$

$$b_n = \frac{\omega_o^2 A_1}{\pi_n}\left[\frac{2 (P - A_o)}{A_1} \sin n t_1 - \Gamma_n\right] \tag{B41}$$

t_1 is defined in Equation (B35) and Γ_n is defined in Equation (B32). For amplitude of motion $A \geq P+2S$

$$b_o = \frac{\omega_o^2 A}{\pi}\left[\frac{A_o}{A_1}\left(t_2 + \pi - t_1\right) + \left(\sin t_2 - \sin t_1\right) + \frac{P}{A_1}\left(t_1 - t_2\right) - \frac{2S}{A_1} t_2\right] \tag{B42}$$

$$b_1 = \frac{\omega_o^2 A}{\pi}\left[\pi + t_2 - t_1 - \frac{2}{A_1}\left(P+2S-A_o\right) \sin t_2 + \frac{2}{A_1}\left(P - A_o\right) \sin t_1 + \frac{1}{2}\left(\sin 2 t_2 - \sin 2 t_1\right)\right] \tag{B43}$$

$$b_n = \frac{\omega_o^2 A}{\pi}\left\{\frac{2}{n}\left[\left(A_o - P\right)\left(\sin n t_2 - \sin n t_1\right) - 2S \left(\sin n t_1\right) + \sigma_n\right\}\right. \tag{B44}$$

t_1 and t_2 are defined by Equations (B35) and (B36) and σ_n is defined as

$$\sigma_n = \left[\frac{\sin (n-1) t_2 - \sin (n-1) t_1}{2 (n-1)} + \frac{\sin (n+1) t_2 - \sin (n+1) t_1}{2 (n+1)}\right]$$

The detailed derivation of the asymptotic solutions for both the freeplay and preload nonlinearities have been presented here. These derivations were included to supplement the discussions of section 2.0 and should be referenced when more detail is required.


DATE
FILME
5-8